

The X-ray Evolution of Merging Galaxies

A. M. Read^{1,2} & T. J. Ponman²

¹ *Max-Planck-Institut für extraterrestrische Physik, Postfach 1603, D-85740, Garching, Germany*

² *School of Physics and Astronomy, University of Birmingham, Edgbaston, BIRMINGHAM, B15 2TT, U.K.*

7 July 2021

ABSTRACT

We present here the first study of the X-ray properties of an evolutionary sample of merging galaxies. Both *ROSAT* PSPC and HRI data are presented for a sample of eight interacting galaxy systems, each believed to involve a similar encounter between two spiral discs of approximately equal size. The mergers span a large range in age, from completely detached to fully merged systems.

A great deal of interesting X-ray structure is seen, and the X-ray properties of each individual system are discussed in detail. Along the merging sequence, several trends are evident: in the case of several of the infrared bright systems, the diffuse emission is very extended, and appears to arise from material ejected from the galaxies. The onset of this process seems to occur very soon after the galaxies first encounter one another, and these ejections soon evolve into distorted flows. More massive extensions (perhaps involving up to $10^{10} M_{\odot}$ of hot gas) are seen at the ‘ultraluminous’ peak of the interaction, as the galactic nuclei coalesce.

The amplitude of the evolution of the X-ray emission through a merger is markedly different from that of the infrared and radio emission however. Although the X-ray luminosity rises and falls along the sequence, the factor by which the X-ray luminosity increases, relative to the optical, appears to be only about a tenth of that seen in the far-infrared. This we believe, may well be linked with the large extensions of hot gas observed.

The late, relaxed remnants, appear relatively devoid of gas, and possess an X-ray halo very different from that of typical ellipticals, a problem for the ‘merger hypothesis’, whereby the merger of two disc galaxies results in an elliptical galaxy. However, these systems are still relatively young in terms of total merger lifetime, and they may still have a few Gyr of evolution to go through, before they resemble typical elliptical galaxies.

Key words: galaxies: individual: (Arp 270, Arp 242, NGC 4038/9, NGC 520, Arp 220, NGC 2623, NGC 7252, AM 1146-270) - galaxies: interactions - galaxies: evolution - galaxies: ISM - galaxies: peculiar - X-rays: galaxies

1 INTRODUCTION

Galaxies were once thought of as ‘island universes’, evolving slowly in complete isolation. This is now known not to be the case. Galaxies interact in a variety of ways with their environment, both with satellite and neighbouring galaxies, and, in the case of galaxies within groups and clusters, with large masses of tenuous hot gas. Collisions and mergers of galaxies are now thought to be one of the most dominant evolutionary mechanisms (Schweizer 1989). Indeed, if events during galaxy formation are counted, there are probably very few galaxies that were not shaped by interactions or even outright mergers (Toomre 1977). The position of a galaxy in Hubble’s (1936) morphological sequence may in

fact depend mainly on the number and severity of merger events in its past history. Pure disc systems, formed from relatively isolated protgalactic gas clouds, appear at one end of the Hubble sequence, the giant ellipticals, possibly produced through mergers of similar spirals, appear at the other, and in between, mergers between galaxies of differing mass produce galaxies with a wide range of bulge to disc ratios.

This *merger hypothesis* discussed above, the idea that elliptical galaxies might be formed from the merger of two disc galaxies, was first suggested by Toomre (1977). The conversion of orbital to internal energy during a close tidal encounter causes the two progenitor systems to sink together and coalesce violently into a centrally condensed system, dis-

rupting any pre-existing discs, and largely randomizing the stellar motions, as shown in many N-body simulations (e.g. Barnes 1988). The problem that ellipticals have central mass densities some $10^2 - 10^3$ times higher than normal spirals has been overcome by the discovery that young merger remnants contain huge central concentrations of molecular gas (Sanders et al. 1986; Sanders et al. 1988a; Scoville & Soifer 1991). Also, elliptical-like luminosity profiles have been discovered in the infra-red underlying the disturbed optical morphology of merging galaxies (Wright et al. 1990). There have been many attempts to disprove the merger hypothesis. Counter-evidence cited includes the fractional abundances of ellipticals in clusters, the colour-luminosity and metallicity-luminosity relationships, radial gradients within ellipticals and with the incidence of globular clusters within ellipticals (see Hernquist 1993). These criticisms can mostly be overcome by appealing to a variety of ideas, such as the growth of substructure in hierarchical cosmogonies, the incomplete nature of violent relaxation, and merger induced star-formation.

Studies of the evolution of merging galaxies have been performed in many regions of the electromagnetic spectrum (Joseph & Wright 1985; Telesco, Wolstencroft & Done 1988; Casoli et al. 1991; Hibbard & van Gorkom 1996), and these are discussed in detail in both Section 2 and Section 5. One region of the electromagnetic spectrum that has been neglected so far though, has been the X-ray.

The *ROSAT* X-ray telescope (XRT), with the Position Sensitive Proportional Counter (PSPC) (Pfeffermann et al. 1986) at the focal plane, offers three important improvements over previous X-ray imaging instruments, such as the *Einstein* IPC. First of all, its spatial resolution is very much improved, the 90% enclosed energy radius at 1 keV being $27''$ (Hasinger et al. 1992). Secondly, the spectral resolution of the PSPC is significantly better ($\Delta E/E \sim 0.4$ FWHM at 1 keV) than earlier X-ray imaging instruments and this allows the derivation of characteristic source and diffuse emission temperatures. Finally, the PSPC internal background is very low ($\sim 3 \times 10^{-5}$ ct s $^{-1}$ arcmin $^{-2}$; Snowden et al. 1994), thus allowing the mapping of low surface brightness emission. The High Resolution Imager (HRI) on the other hand, because of its excellent spatial resolution ($\approx 5''$) and relative insensitivity to diffuse emission, is an ideal instrument for further investigation into the point source populations.

Furthermore, as *ROSAT*'s energy band is relatively soft compared to that of the *Einstein* IPC (and to other previous instruments), the hot halos now known to exist around many nearby normal galaxies (e.g. Bregman & Pildis 1994; Wang et al. 1995; Read, Ponman & Strickland 1997), may be observable within these more distant, though more active systems. Indeed as shall be discussed later, a hot halo is known to exist around the merging galaxy pair, the *Antennae* (NGC 4038/9) (Read, Ponman & Wolstencroft 1995).

In the *ROSAT* band, it appears that the X-ray emission from normal spiral galaxies is made up of a complex mix of sources. Both stellar sources such as low- and high-mass X-ray binaries, cataclysmic variables and normal main sequence stars, and interstellar sources such as supernova remnants (SNRs) and the hot phases of the ISM, contribute to the total X-ray emission. The merger of two similar spiral galaxies may lead to additional sources of X-ray emission. The advances in instrumentation discussed above should al-

low a substantial improvement in our knowledge of the complex X-ray properties of interacting galaxies over what was possible with *Einstein* (see Fabbiano 1989 and references therein). The variation in X-ray emission with merger stage and position can be compared with corresponding multi-wavelength results to reveal new clues as to how the tidal forces trigger star formation, and to constrain the nature and duration of the activity which ensues.

Studies of the nearest, and therefore best resolved, interacting systems are especially important, and many of the most attractive targets have been observed by *ROSAT*. We have undertaken a programme of *ROSAT* PSPC and HRI observations of a carefully chosen chronological sequence of merging galaxies in order to study the evolution of their X-ray properties through the merging process. We have combined our own *ROSAT* data with other archival *ROSAT* data and with individual studies published recently. Where possible, we have attempted to analyse these systems in a uniform manner. In particular we have carefully separated point sources from what appears to be diffuse X-ray emission, and have determined the spectral properties of each.

In the present paper we describe the analysis we have performed, and present the basic results for each of our sample systems in turn. In some cases, we are able to compare with previous authors' results from the same data, but in many instances our analysis is the first reported *ROSAT* analysis, and in some cases it represents the first picture of the X-ray emission from an imaging telescope.

The plan of this paper is as follows. After some comments (Section 2) on the selection of the sample, Section 3 describes the observations and the data reduction methods. The results for each galaxy are presented in Section 4, together with notes on the individual systems. In Section 5, we comment on the range of galaxy properties which emerges, and discuss the X-ray evolution of the sample as a whole. Finally, in Section 6 we present our conclusions.

2 THE MERGING GALAXY SAMPLE

The basic problem with a chronological study is to establish the ordering of the sample. The most famous chronological sequence of merging galaxies is undoubtedly the 'Toomre sequence' (Toomre 1977), containing the 11 best examples of ongoing mergers from the New General Catalogue of Nebulae and Clusters of Stars (NGC). These systems appear, when ordered chronologically, to range from well separated, strongly interacting systems, apparently destined to eventually merge, through systems in the throes of merging, to well merged systems. This sequence has formed the basis for other evolutionary studies made at other wavelengths, as discussed below, and indeed, forms the basis for the selection of the present sample.

Relevant studies at other wavelengths were, until very recently, rare. Joseph and Wright (1985) studied highly disturbed systems in which the two disc galaxies had lost their individual identities and appear as a single coalesced object, the primary morphological indication of which is the presence of the two tidal tails. Dynamical simulations (Toomre and Toomre 1972) suggested that the tails will persist for $\sim 10^9$ years, and the faintness of these tails, together with the degree of coalescence, were used as indicators of rel-

ative merger age. Comparing the infrared luminosities of these galaxies they found that the two youngest and two oldest systems were less luminous than the four ‘middle-aged’ systems, suggesting that merging galaxies undergo a phase of starburst activity of characteristic luminosity $\sim 10^{12} L_\odot$. Another useful indicator of the progress of a starburst was found by Telesco, Wolstencroft & Done (1988); for comparably sized interacting galaxies, the dust colour temperature and the interaction strength is greatest for the pairs with the smallest separation. Furthermore, Casoli et al. (1991), while studying the molecular gas content within a series of merging systems, discovered that the far-infrared colour temperature, the L_{FIR}/L_B ratio and the $L_{FIR}/M(H_2)$ ratio all evolve along the sequence, increasing in the early stages of the collision, reaching a climax, and then decreasing to values typical of ellipticals.

Much more recently, Hibbard & van Gorkom (1996) have presented H I, H II, and R-band observations of an evolutionary sequence of merging systems, again taken primarily from the Toomre sequence. Their five systems, four of which appear in the Toomre sequence, and three of which appear in this present paper, span a large range in merger stage, unlike the work of Joseph & Wright (1985) discussed above, where only middle stage mergers were considered. Much of Hibbard & van Gorkom’s (1996) work is very relevant to the present paper, and many of their results are used in our discussion (Section 5). They find that, moving from early to late-stage mergers, a larger fraction of the neutral hydrogen is found outside of the optical confines of the system, and in the last stage, all of the H I is found in the tails, with none in the central regions. They suggest that the interaction-induced relaxation causes most of the atomic gas within the original discs to compress, condense, form stars and/or shock-heat to X-ray temperatures, any residual atomic gas remaining in the remnant being heated via the resultant starburst.

In order to make the establishment of a reliable chronological ordering as easy as possible, the systems were carefully chosen on the basis of both close attention to the work of the previous authors’ described above, especially Toomre’s (1977) sequence, and the following important criteria:

- All the systems contain, or appear to have evolved from, two spiral galaxies of fairly equal mass.
- A wide range of merger stages, wider in fact than the Toomre sequence, from completely detached to fully merged systems, is covered.
- All the systems are infrared and radio bright, indicating the presence of unusual star-formation activity.
- Low absorbing columns ($1.2 - 5.2 \times 10^{20} \text{ cm}^{-2}$) exist in the directions of all these systems, maximizing the sensitivity to soft X-ray emission.
- All the systems are large enough for worthwhile spatial resolution to be achieved with the PSPC, and for detailed mapping of point sources with the HRI.
- Much additional multiwavelength information is available for all these systems.

Optical morphology (especially the appearance of tidal tails, and the proximity of the two nuclei) has been used as the primary measure of merger stage, but this has been supplemented with the following additional indicators.

Toomre & Toomre (1972) have shown that proper tail construction requires that the perturbing mass be at least comparable to the perturbed, and that therefore, major tidal tails should protrude from both of two interacting discs of roughly equal dimensions as in NGC 4676 (the *Mice*) and NGC 4038/9 (the *Antennae*). For systems where the central parts of the galaxy have not yet merged, tail length seems the best indicator of age, increasing with time (Toomre & Toomre 1972), although tail length also increases with the closeness of the encounter. Once the nuclei of the galaxies have merged, the tails begin to diffuse away, and so using the morphology of the systems to order them chronologically comes down to a combination of tail length, tail faintness and degree of coalescence of the nuclei.

Listed below, in chronological order, are the eight systems within the sample, selected on the basis of the above considerations. Optical pictures of the eight systems are shown in figure 1. All are taken from the digitised sky survey, the southern systems from the U.K. Schmidt plates and the northern systems from the Palomar Schmidt plates.

Arp 270 (NGC 3395/6) consists of two low IR-flux galaxies, obviously involved in some sort of interaction, though the lack of tidal tails is suggestive of them not having properly encountered one another yet. This system is in fact a pre-Toomre sequence system.

Arp 242, the *Mice* (NGC 4676), occurs second in the Toomre sequence and, though it appears rather similar to Arp 270, the presence of tidal tails and an obvious bridge between the two galaxies, together with an increase in IR activity, indicates that the galaxies have begun to interact, and have passed each other.

NGC 4038/9, the *Antennae* (Arp 244), is a classic example of an interacting system with two equally long tails and distinct central masses. Although it occurs first in the Toomre sequence, CO (Stanford et al. 1990), radio (Hummel & van der Hulst 1986) and X-ray observations (Read et al. 1995) indicate that the discs have begun to merge, and the *Antennae* therefore should really be placed sometime after the *Mice*.

NGC 520 (Arp 157), seventh in the Toomre sequence, and classified as an intermediate-stage merger by Hibbard & van Gorkom (1996), is as radio and infrared bright as the *Antennae*, and has two smaller tails as well as two nuclei and two velocity systems in its spectra, indicative of a young merger.

Arp 220, one of the superluminous IRAS galaxies, is a prototypical merger. It is the brightest of the sample across the whole of the electromagnetic spectrum (except for the optical). Huge H α filaments exist (Heckman, Armus & Miley 1990), suggestive of vigorous starburst activity. Two distinct (though very close) nuclei are visible in the infrared (Majewski et al. 1993).

NGC 2623 (Arp 243), appearing eighth in the Toomre sequence, is, like Arp 220, a superluminous IRAS galaxy, and is also very bright in the radio. Very long tails are visible but the central masses have become indistinguishable. Only one true nucleus is thought to exist.

NGC 7252 (Arp 226), the *atoms for peace* galaxy, is the prototypical merger remnant, and is the last system within the Toomre sequence. It has two equally long, very faint tails emanating from a disturbed, double motion

spheroidal body whose mean light distribution closely follows the de Vaucouleurs $r^{1/4}$ law, typical of ellipticals.

AM 1146-270, beyond the end of the Toomre sequence, is a spheroidal galaxy with a small tail-like structure, appears to be the site of a great deal of recent star formation, hence the many blue knots surrounding its nucleus.

Table 1 lists the sample systems together with the following basic properties. Distances are, where possible, taken from Tully (1988). These are based on $H_0 = 75 \text{ km s}^{-1} \text{ Mpc}^{-1}$, and assume that the Galaxy is retarded by 300 km s^{-1} from universal expansion by the mass of the Virgo cluster. For the more distant galaxies, distance values are either taken from Condon et al. (1990), where the same H_0 and Virgocentric flow correction is used, or are calculated from the group-flow-corrected radial velocities given in the Second Reference Catalog of Bright Galaxies (RCBG) (de Vaucouleurs, de Vaucouleurs & Corwin 1976), using a H_0 of $75 \text{ km s}^{-1} \text{ Mpc}^{-1}$. AM 1146-270's radial velocity is taken from Sekiguchi & Woltencroft (1993).

Optical (B) luminosities for all the systems in the sample are calculated as in Tully (1988), i.e. as a re-expression of the absolute magnitude, itself following from the blue apparent magnitude B_T , and the distance D :

$$\log L_B(L_\odot) = 12.192 - 0.4B_T + 2 \log D.$$

Blue apparent magnitudes are, again where possible, taken from Tully (1988). Values for the more distant systems are taken from RCBG (de Vaucouleurs, de Vaucouleurs & Corwin 1976) and from NGC 2000.0 (Dreyer 1988) (the value for AM 1146-270 is taken from Smith & Hintzen 1991)).

FIR luminosities are calculated from IRAS 60 and $100 \mu\text{m}$ fluxes (taken from the IRAS Point Source Catalogue) using the expression

$$L_{\text{FIR}} = 3.65 \times 10^5 [2.58S_{60\mu\text{m}} + S_{100\mu\text{m}}] D^2 L_\odot,$$

(e.g. Devereux & Eales 1989). Here D is the distance in Mpc and $S_{60\mu\text{m}}$ and $S_{100\mu\text{m}}$ are the IRAS 60 and $100 \mu\text{m}$ fluxes (in Janskys). Also given in table 1 are the infrared to blue luminosity ratio, L_{FIR}/L_B , and the dust colour temperature, S_{60}/S_{100} . These two infrared indicators are the two suggested by previous studies (Joseph & Wright 1985; Telesco et al. 1988) to be worthwhile indicators of starburst activity, and it can be seen that they rise and fall along the chronological sequence in just the way one might expect if a burst of star formation were triggered during a merger. Finally, included also in Table 12 are the radio luminosities from Condon et al.'s (1990) 1.49 GHz atlas of the *IRAS* bright galaxy sample, supplemented in the cases of Arp 242 and NGC 7252 (upper limit), with the luminosities (converted to $H_0 = 75 \text{ km s}^{-1} \text{ Mpc}^{-1}$) from Heckman's (1983) study.

3 OBSERVATIONS AND DATA REDUCTION

Both PSPC and HRI data have been analysed within this study, and the methods of data extraction and reduction for both types of data are described below. All of the HRI data and the PSPC data for three of the systems (NGC 4038/9, NGC 2623 and AM 1146-270) were obtained through our

own pointed observations. The remaining PSPC datasets were obtained from the UK *ROSAT* Data Archive Centre at the Department of Physics and Astronomy, Leicester University U.K.

3.1 PSPC Observations and Data Reduction

All of the PSPC datasets have been analysed in essentially the same way using the STARLINK *ASTERIX* X-ray analysis system. This method is described below, and in greater detail in Read et al. (1997). Departures from this standard procedure are described in detail in the notes on the individual systems (sections 4.1–4.8). In every case, the target system in question lay at the centre of the PSPC field, thus minimizing the effects of vignetting and blurring.

Once the data were 'cleaned' of high background periods ($\approx 2 - 3\%$ of the data), they were binned into a (0.1–2.3 keV) spectral image (or 'data cube') of size approximately twice that of each system. An annulus situated outside the PSPC central support ring, and with the bright sources within it removed, was formed from the data, and this background region was, together with knowledge of the PSPC vignetting function, used to construct a background model. When this was subtracted from the data cube, the resultant background-subtracted data cube could be used to form images in different spectral bands.

PSS (Allan, Ponman & Jeffries, in preparation), a point source search program which uses a likelihood technique to search for enhancements above the background, was used to search for point-like emission within these images. The basic method of PSS involves a comparison of the input dataset (in this case, the image) with a model, comprising of a background and a scaled PSF. The positions of the detected point sources, i.e. those with a significance $\geq 4\sigma$ (except where stated in the text), were cross-correlated with a variety of stellar and non-stellar catalogues, including the SIMBAD catalogue and the *Einstein* and IRAS point source catalogues.

As in Read et al. (1997), we attempted to separate the diffuse from the source emission by removing data from the background-subtracted data cube at the position of each PSS source over a circle enclosing 93% of the energy of a 0.5 keV point source (as all the sample systems subtended small angles, this extraction radius was never greater than about half an arcminute). The remaining data were then collapsed into a spectrum and corrected for vignetting effects and exposure time. To account for the diffuse flux lost in the source removal process, the diffuse spectrum was renormalised using a 'patched' image, where the 'holes' left after source removal were filled by bilinear interpolation.

This method of separating the point source emission from the diffuse emission did not, in general, work as well as in Read et al. (1997). This is not surprising as the systems in the present study are at much greater distances than those studied in Read et al. (1997), and both limitations on sensitivity and on resolution have had a more serious impact.

As in Read et al. (1997), source spectra were binned directly from the raw data from circles of the same size as those used in the source removal procedure above. To obtain true *source* spectra however, both the local true background flux, obtained by scaling the background emission from source-free regions of the field using knowledge of the

Figure 1. The merging galaxy sample: A) Arp 270, B) Arp 242, C) NGC 4038/9, D) NGC 520, E) Arp 220, F) NGC 2623, G) NGC 7252, H) AM 1146-270

System	Other names	Distance (Mpc)	$\log L_B$ (erg s $^{-1}$)	$\log L_{FIR}$ (erg s $^{-1}$)	L_{FIR}/L_B	S_{60}/S_{100}	$\log L_{rad}$ W hz $^{-1}$
Arp 270	NGC 3395/6	28	44.08	43.61	0.335	0.486	21.93
Arp 242	NGC 4676	88	44.06	44.09	1.069	0.534	22.18
NGC 4038/9	Arp 244	25	44.19	44.20	1.026	0.516	22.64
NGC 520	Arp 157	28	43.87	44.15	1.900	0.651	22.24
Arp 220	UGC 9913	76	43.96	45.52	36.04	0.884	23.39
NGC 2623	Arp 243	78	43.78	44.87	12.28	0.862	22.85
NGC 7252	Arp 226	63	44.28	44.00	0.526	0.565	<22.78
AM 1146-270		25	42.93	42.55	0.416	0.590	-

Table 1. The merging galaxy sample, listed in order of evolutionary age. Sources for the tabulated parameters are given in the text.

PSPC vignetting function, and the local diffuse flux, calculated by scaling the integrated spectrum of the diffuse emission with an estimate of the fraction of the diffuse flux underlying each source, had to be removed from each source spectrum.

So, in summary, three types of spectrum were formed from each dataset:

- An **integrated Spectrum** was extracted from a circular area of diameter slightly greater than the optical diameter of each system. Although particle and cosmic X-ray backgrounds were removed, no sources were excluded. Standard spectral models (power law, bremsstrahlung and Raymond and Smith (1977) hot plasma) were used in the fitting. Even though these spectra contain emission from

everything around each system's position, including galactic sources, galactic diffuse emission, and foreground and background sources (both Galactic and extragalactic), some of the resultant spectral fits are very acceptable. The net number of counts, the χ^2 values, number of degrees of freedom (n.d.o.f.), and the integrated X-ray luminosities (0.1–2.0 keV) inferred from the spectral fitting, are shown in each of Tables 3 to 10.

- A **Diffuse spectrum** was extracted, using the method described above, from an area the same size as that used for the integrated spectrum. The correctly normalized (0.1–2.0 keV) X-ray luminosities of each system's diffuse emission are tabulated in Tables 3 to 10, along with the net diffuse counts and the results of the spectral fits (using again the same models as those used above). Because of low count rates, χ^2 fitting could only be used in the case of the *Antennae*. In all other cases, a maximum likelihood criterion, which allows for the Poissonian nature of the data, had to be used. Unfortunately, when using likelihood fitting, the absolute value of the statistic is not informative (and hence we have not given it). The Cash statistic (Cash 1979) can be used however, to compare the relative quality of different fits, and to derive confidence intervals for model parameters, since *differences* in the value of the Cash statistic from one model to another, are distributed in the same way as χ^2 . Furthermore, only the freezing of certain parameters at sensible values led to acceptable fits in a few cases (these are indicated by a bracketed 'F'). All these results are described in detail in Sections 4.1 to 4.8. Because of the large distances involved, many of these systems' diffuse emission spectra will be complicated, involving some genuinely diffuse gaseous emission, and some contribution from both unresolved point sources and from 'stumps' left in the subtraction of the bright sources. Hence, we attempted, where possible, to fit a 2-component model to the diffuse spectrum, comprising of a Raymond and Smith hot plasma (representing the truly diffuse gas) and a highly absorbed hot (10 keV) component (representing unresolved sources). These results are also described in more detail later in the notes on the individual systems.

- **Individual source spectra** were extracted as described above. Sources known not to be connected with the galaxy were excluded from the analysis, as were sources that lay outside both the optical emission and any diffuse X-ray emission. The results of the spectral analysis of all the sources within each system are tabulated below in each of the individual galaxy sections. The point source spectra generally contained low numbers of counts, and Gaussian statistics could not be assumed. A maximum likelihood criterion, as described above, was used.

3.2 HRI Observations and Data Reduction

The three HRI datasets (NGC 520, NGC 2623 and NGC 7252) were analysed in exactly the same way, again using the STARLINK ASTERIX X-ray analysis system. In each case the data were first binned into a $0.4^\circ \times 0.4^\circ$ image with a 3" resolution, thus exploiting the HRI's superior spatial resolution. Background subtraction of HRI data, although significantly easier than of PSPC data, is still non-trivial, and two methods were utilised, which were compared both with each other and with the mean HRI background

System	BR	BR
	0.3 keV	3.0 keV
NGC 520	6.47×10^{-4}	3.50×10^{-4}
NGC 2623	4.54×10^{-4}	2.31×10^{-4}
NGC 7252	7.11×10^{-4}	4.99×10^{-4}

Table 2. Counts-to-flux Conversion factors for the *ROSAT* HRI detector for the three individual HRI datasets and for two separate thermal bremsstrahlung models. The values are corrected for Galactic absorption and are in units of $10^{-11} \text{ erg cm}^{-2} \text{ s}^{-1} \text{ cts}^{-1}$.

rate ($\approx 1.1 \times 10^{-6} \text{ ct s}^{-1} \text{ arcsec}^{-2}$; David et al. 1993). Firstly, a polar profile of the data was formed about the centre of the system, with radial bins of width 0.001° . This was seen to level out at large radius to a constant background level. The second method involved an evaluation of the mean value, once all the bright features had been removed from the data. The background values obtained from the two methods agreed well in all three cases. These values were subtracted from the raw data (over such a small area, the vignetting is essentially flat, and can be ignored).

The resultant image was then exposure corrected, and searched for sources, again using PSS. Again, a detection threshold of 4σ was assumed. Images, smoothed on many different spatial scales (from 3" to 18"), were formed to search for extended low-surface brightness features.

Count rates of the detected point sources within the three HRI datasets were converted into fluxes (and then into luminosities), assuming 0.3 keV and 3.0 keV thermal bremsstrahlung models. HRI conversion factors for both models from number of counts into fluxes (taking into account the different exposure times and Galactic foreground N_H values) are given in Table 2.

Although the spectral response of the HRI is rather poor, it is thought (Fraser 1992) that the ratio of the number of counts in channels 1–5 to the number of counts in channels 6–11, used by Wilson et al. (1992), does seem the most sensitive energy indicator that can be constructed. The above analysis was also repeated for data within these two energy bands.

4 RESULTS

The following eight subsections describe the results of the analyses of *ROSAT* PSPC and, where applicable, HRI data of the sample systems. Where the analysis technique differs from that described in Section 3 this is noted in the text.

Within each of Sections 4.1 to 4.8, a table is given, showing the main results of the analysis of each set of *ROSAT* PSPC data. The results of the spectral analyses of each of the three types of spectra formed as described in Section 3 (an integrated spectrum, a diffuse spectrum and individual source spectra), are given. The number of counts, plus the statistical uncertainty, contained within each spectrum are given, together with the results of the best spectral fit to each spectrum. A quoted photon index indicates that the best fit is a power law model, whereas if instead, a temperature is given, the best fit is either a Raymond & Smith

hot plasma model (if the metallicity is quoted), or it is a bremsstrahlung model (if no metallicity is quoted). Where χ^2 -fitting has been used (in fitting most of the integrated spectra plus a small number of other high-count rate cases), the values of the χ^2 statistic are given together with the number of degrees of freedom. The (0.1–2.0 keV) X-ray luminosities tabulated are those *escaping* from the system in question, i.e. before absorption in our own galaxy. Also given in each case is the value of L_x (diffuse+sources), the sum of the diffuse X-ray luminosity and each of the individual source luminosities.

Unless otherwise stated, we also present for each source a PSPC image showing contours of background-subtracted, exposure-corrected X-ray emission in the 0.1–2.3 keV band, superimposed on an optical image of the system. These X-ray images have a resolution of 5" and have been lightly smoothed with a Gaussian of standard deviation 10" to suppress noise. The contour levels increase by factors of two from 7.2×10^{-4} ct s⁻¹ arcmin⁻².

4.1 Arp 270

Arp 270 (also VV 246; Vorontsov-Velyaminov, 1959) is composed of two galaxies, thought to be of comparable masses (Davis & Sequist 1983), NGC 3395, to the west, and the somewhat smaller, more irregular galaxy, NGC 3396, to the east. The angular separation of their nuclei ($\approx 90''$) corresponds to a separation of about 12 kpc at the distance of 28 Mpc assumed within this paper. In the far-infrared, they appear as a strong, though unresolved source (Soifer et al. 1987), and in the UV, they are noted in the KISO catalogue (Takase & Miyauchi-Isobe 1987) as an interesting pair of UV-excess galaxies. Many radio continuum studies have been made, the most noteworthy being that of Huang et al. (1994), who find that the radio emission in each galaxy comes predominantly from that part of each galaxy near its companion galaxy. Whereas NGC 3396 shows two strong radio peaks and one weak one, its partner has a much more complex structure, with six or more peaks in the north-eastern part of the galaxy alone. A clear bridge between the two galaxies is also seen in the radio, roughly coincident with the optical.

Arp 270 has been observed in X-rays previously to *ROSAT*, with the *Einstein* IPC. The *Einstein* image (Fabian et al. 1992) shows very little structure, what there is appearing to be centred on NGC 3395. Suggestions of extensions are also visible to the north-west and south-west of the system.

The *ROSAT* image (Fig. 2) shows far more structure than seen with *Einstein*. Emission is seen to come from both galaxies, and this emission appears to be enshrouded in more diffuse emission. The X-ray feature associated with the western galaxy (source A; see Table 3) appears to be centrally positioned and lies less than 2" from the position given in the Third Reference Catalog of Bright Galaxies (RC3) (de Vaucouleurs et al. 1991). Source B however, does appear, like the radio emission discussed above, to emanate from a position in NGC 3395 nearer to its companion galaxy (X-ray source B lies some 27" from the RC3 position of NGC 3396. As Huang et al. (1994) point out, this is not expected from dynamical simulations. Instead, the gas should be forced through the tidal interaction towards the nuclear regions of

Figure 2. Contours of (0.1–2.3 keV) X-ray emission shown superimposed on an optical image of Arp 270. Contour levels increase by factors of two from 7.2×10^{-4} ct s⁻¹ arcmin⁻².)

each galaxy, and be compressed into star-formation. This process however, as Huang et al. note, will take some time, and the star-formation may well begin before the gas reaches the nuclear regions. Non-nuclear bursts of star-formation can occur in the collision between two gas-rich spiral galaxies, when a burst of massive star-formation is first triggered in the overlapping/interpenetrating regions of the galaxies (Jog & Solomon 1992). This overlapping region will at first be the very outer discs of the two galaxies. In the case of Arp 270 though, it appears that this very initial phase may be nearly over, as gas is now seen close to the nuclear regions, i.e. the forcing of gas through the interaction towards the galactic nuclei has begun. The fact that, in the case of NGC 3396, this hot gas is seen only close to the nucleus, not yet within it, may indicate that this second phase, the tidal forcing of gas towards the two nuclei, may have only just begun. Furthermore, there is quite a good correlation between the X-ray contours in Fig. 2 and the radio data of Huang et al. (1994) – both the tentative X-ray ‘bridge’, seen apparently connecting the two galaxies, and the radio bridge appear to connect the two systems along the southern edge of the optical bridge.

Both source spectra are best fit with low-temperature, absorbed plasma models, suggestive of the emission from both regions being due to hot gas, rather than to evolved stellar components. The fact that no evidence was found in the radio for an active galactic nucleus in either galaxy, and that the radio spectra of the galaxies are relatively flat (at low frequencies) (Huang et al. 1994), indicative of a good deal of supernova activity, adds credence to the hot gas idea.

The two other detected sources in the field, the strong point-like source to the north of NGC 3396, and the weaker source within the X-ray ‘tail’ to the south-west of NGC 3396, appear to explain the suggested extensions tentatively seen in the *Einstein* image. The northern source is unlikely to have anything to do with the system, and is most probably

a background quasar, its best spectral fit being a power-law fit with a photon index, $\alpha = 2.3 \pm 0.5$, consistent with the mean spectrum of quasars in the *ROSAT* band (2.2 ± 0.2 ; Branduardi-Raymont et al. 1994; Roche et al. 1995). The X-ray feature to the south-west of NGC 3395 however, may well be associated with the system. The radio observations of Huang et al. (1994) do show that some emission has diffused beyond the optical edge of the galaxy within this region, perhaps indicative of previous supernova outbursts. This would help to explain the existence of hot X-ray emitting gas also. The number of counts within this region make it difficult to constrain its spectral properties.

The ‘diffuse’ spectrum of Arp 270 as a whole appears severely contaminated, both by unresolved point sources, and by ‘stumps’ of source emission left in the source-subtraction procedure (see Section 3.1). This is reflected in the rather wide confidence errors quoted on the best fit values in Table 3 (remember, no goodness of fit can be quoted as a maximum likelihood technique had to be used because of the small number of counts). As discussed in Section 3.1, we attempted to fit a two-component model to the diffuse spectrum, comprising a Raymond & Smith hot plasma (representing the hot gas), and a highly absorbed hot (10 keV) component (representing the source contamination component). This two-component fit suggests, as shown in Table 3, that approximately two-thirds of the ‘diffuse’ emission may be truly diffuse gas at a very low (< 0.2 keV) temperature, while the remaining third of the emission can be accounted for in terms of highly absorbed, hard (10 keV) sources. An F-test shows that the improvement in fit quality to the ‘diffuse’ spectrum from including the second component is significant at over 99% confidence.

4.2 Arp 242

One of the original systems presented by Toomre & Toomre (1972) as a classic example of a pair of galaxies undergoing tidal interaction is Arp 242 (the *Mice*). Also known as NGC 4676, this system lies second in the proposed evolutionary sequences of both Toomre (1977) and Hibbard & van Gorkom (1996), as well as in the present work. Recent kinematical work (e.g. Mihos, Bothun & Richstone 1993) has strengthened further the tidal interpretation of the *Mice*’s structure, and it is now generally agreed that both galaxies, in the throes of a prograde encounter, have their northern edges moving away from us, such that NGC 4676a’s tail is on the very furthest side, swinging away from us, and NGC 4676b is rotating clockwise, its northeastern portion, the closest to us (Hibbard & van Gorkom 1996). Hibbard & van Gorkom (1996) find these kinematics in general agreement with their H I velocity data. What discrepancies they do see allow them to derive a mass ratio of 2:1 for NGC 4676b:NGC 4676a.

Both the northern galaxy (NGC 4676a) and the southern galaxy (NGC 4676b) appear to have shapes and colours consistent with those of early-type spirals, though the disc regions are strongly distorted or absent. Both tails, although bluer than the galaxies’ central colours, are in agreement with the colours of outer-disc regions (Schombert, Wallin & Struck-Marcell 1990). They account for 16% of the total $H\alpha$ emission, are quite luminous, containing one-third of the to-

tal R-band luminosity of the system, and have a high atomic gas content (Hibbard & van Gorkom 1996).

The northern galaxy appears to exhibit a $6.6h^{-1}$ kpc plume of $H\alpha$ along its minor axis, and the southern galaxy possesses an ionized gas bar, as produced in Barnes & Hernquist’s (1991, 1996) merger simulations, offset with respect to the stellar bar (Hibbard & van Gorkom 1996). Angular momentum transfer between the two bars is able to force large amounts of gas towards the galactic centre.

Arp 242 has never been observed in X-rays previously. The X-ray image (Fig 3) shows rather an amorphous X-ray structure. The one source detected (labelled ‘A’) lies further than the *ROSAT* rms attitude uncertainty ($\approx 6''$; Hasinger et al. 1992) from the nuclei of either galaxy, lying approximately $40''$ south of NGC 4676a and $20''$ west of NGC 4676b. It may be, that the source is actually associated with the contact region between the two galaxies, and is either collisionally heated gas or possibly due to enhanced star formation taking place in the dense molecular clouds in the contact region. Unfortunately, due to lack of counts and limitations on resolution, very little can be said about the spectral properties of the source, or its true position.

Leaving aside this source for the moment, the remainder of the emission does seem, in general, to follow the optical ‘heads’ of the galaxies, running from the south-east to the north-west. The little ‘spur’ to the south-west, though interesting, is probably spurious, or if not, unlikely to be associated with the system. The feature to the north-west however, may well be associated with the NGC 4676a $H\alpha$ plume (Hibbard & van Gorkom 1996) extending in the same direction. The correlation of $H\alpha$ and X-ray features extending along the minor axis of galaxies, is often a good indicator of a starburst-driven galactic wind taking place, both the $H\alpha$ and the X-ray emission being due to clouds (of different densities) being shocked by the hot, fast wind from the galactic nucleus (Heckman, Lehnert & Armus 1993). While the fitted temperature to the diffuse emission spectrum is in very good agreement with fitted temperatures of more nearby, known, starburst winds (Heckman 1993; Read et al. 1997), the small number of counts, make it impossible to be confident of this result.

4.3 NGC 4038/9

The *Antennae*, NGC 4038/9 (also Arp 244) is perhaps the classic example of a pair of galaxies in gravitational interaction, with spectacular tails spanning nearly 150 kpc. It has been the study of many dynamical models (Toomre & Toomre 1972; Barnes 1988), and the basic validity of these models has been confirmed by studies in neutral (van der Hulst 1979) and ionised (Amram et al. 1992) hydrogen gas. $H\alpha$ emission knots (Rubin, Ford & Dooderico 1971), coincident with powerful radio features (Hummel & Van der Hulst 1986; Wolstencroft 1988) are found throughout the central parts of both galaxies, and Van der Hulst (1979) showed that about 70% of the H I in the system lies in the optical tails. Both infrared (Bushouse & Werner 1990; Vigroux et al. 1996) and CO (Stanford et al. 1990) observations indicate that both the nuclei, and the contact region between the two galaxies, are likely to be sites of very active star formation.

The results of the *Einstein* observation of the *Anten-*

Source Spectrum Analysed		Net Counts	$\log L_X$ erg s $^{-1}$ (0.1–2.0 keV)	Best Spectral Fit Results				
R.A. (2000.0)	Dec (2000.0)			column 10 20 cm $^{-2}$	photon index	temp. keV	Z (solar)	χ^2 (n.d.o.f)
Integrated		396 \pm 37.4	40.48	7.76 $^{+2.94}_{-2.03}$	3.11 $^{+0.44}_{-0.43}$			20.16 (19)
‘Diffuse’ 1-component fit			40.04	5.10 $^{+5.46}_{-3.18}$		2.56 $^{+9.51}_{-0.30}$	0.00 $^{+0.38}_{-0.00}$	
‘Diffuse’ 2-component fit		168 \pm 34.2	(RS) 40.01 (Br) 39.75	2.01 $^{+72.1}_{-0.48}$ 150 $^{+93.4}_{-71.7}$		0.17 $^{+0.11}_{-0.11}$ 10 (F)	1.30 $^{+5.42}_{-0.44}$	
Source A	10 49 49.58	+32 58 51.6	112 \pm 13	39.92	6.49 $^{+3.02}_{-1.78}$		0.57 $^{+0.21}_{-0.13}$	
Source B	10 49 54.53	+32 59 16.9	95.3 \pm 12	39.81	4.91 $^{+2.30}_{-1.60}$		0.63 $^{+0.30}_{-0.17}$	
Best ‘Diffuse’ + sources				40.49				

Table 3. The results of the PSPC spectral analysis of Arp 270. Tabulated luminosities are those escaping from the system. Only the best model fit is shown. Errors on the spectral fit parameters are 1σ for one interesting parameter.

Source Spectrum Analysed		Net Counts	$\log L_X$ erg s $^{-1}$ (0.1–2.0 keV)	Best Spectral Fit Results				
R.A. (2000.0)	Dec (2000.0)			column 10 20 cm $^{-2}$	photon index	temp. keV	Z (solar)	χ^2 (n.d.o.f)
Integrated		53.8 \pm 19.0	40.76	4.37 $^{+5.53}_{-4.37}$		0.10 $^{+0.13}_{-0.10}$	0.05 $^{+118}_{-0.05}$	41.78 (18)
Diffuse		31.2 \pm 18.4	40.66	0.00 $^{+2.63}_{-0.00}$		0.35 $^{+0.39}_{-0.19}$	0.04 $^{+0.45}_{-0.04}$	
Source A	12 46 09.96	+30 43 20.8	17.5 \pm 5.5	40.22	66.2 $^{+121}_{-63.3}$		0.24 $^{+0.58}_{-0.15}$	
Diffuse + sources				40.80				

Table 4. The results of the PSPC spectral analysis of Arp 242. Tabulated luminosities are those escaping from the system. Only the best model fit is shown. Errors on the spectral fit parameters are 1σ for one interesting parameter.

nae (Fabbiano & Trinchieri 1983) were rather inconclusive, though the emission was seen to be extended, and contained a soft X-ray contribution. Harder emission and a possible hard point source at the contact region were also seen. The *ROSAT* PSPC observation sheds far more light on to the matter, and full details of the observation, the analysis and the results, are given in Read et al. (1995), though a summary is presented below.

The *ROSAT* PSPC data were processed initially in a manner very similar to the method presented here, though further, more sophisticated techniques were used in the latter stages of the analysis (see Read et al. 1995). Using a maximum entropy reconstruction technique (Gull 1989; Skilling 1989), a number of discrete components to the X-ray emission were identified (A–G; see Table 5 and Fig. 4). Many of these have counterparts at other wavelengths; B and D are associated with the northern (NGC 4038) and the southern (NGC 4039) nuclei respectively. Their properties, the facts that they are best fitted with low-temperature and relatively low-column plasma models, that there are offsets between the X-ray positions and the radio positions, and that it is known that there is a great deal of supernova activity taking place at these sites, suggest that they are bubbles of hot extranuclear gas, rather than the central starbursts themselves. Features A, C, and possibly E have massive $H\alpha$ knots and radio features as counterparts, and are likely to be giant H II regions.

Nearly half of the *Antennae*’s X-ray flux appears diffuse, and a two-component spectral fit (see Table 5), indicates that almost all of it is genuine, hot (4×10^6 K), low-metallicity gas (the rest being due to unresolved sources), with a total mass perhaps exceeding $10^9 M_\odot$. The bulk of this emission appears to envelope the entire optical system, except for the tidal tails. An enhancement (accompanied by a rise in temperature to over 10^7 K) is seen in this diffuse emission at the contact point between the two galaxies, where it is believed the two discs are colliding. This may be due to gas heated by the collision, or to triggered star-formation in the vicinity. Of great interest are the two elongated structures extending to the northwest and to the southwest, extending from the galactic discs to radii of ~ 30 kpc, and culminating in symmetrically-positioned, apparently point-like, sources (P and Q). These streamers most likely indicate the existence of galactic winds, their normal bipolar structure possibly having been disturbed by the rapid dynamical evolution of the system (see Section 5.3 for further discussion of this). Containing $\approx 10\%$ of the total hot gas present, these streamers could represent a significant loss in mass and energy from the system.

The point sources at the ends of the two arms are a real puzzle. The sources could be related to the arms if they were massive ($\sim 10^8 M_\odot$) objects, ejected from the galactic nuclei (see Saslaw, Valtonen & Aarseth 1974), the ejection process giving rise to the juxtaposed ‘wakes’ of hot gas. How-

Figure 3. Contours of (0.1–2.3 keV) X-ray emission shown superimposed on an optical image of Arp 242. Contour levels increase by factors of two from $7.2 \times 10^{-4} \text{ ct s}^{-1} \text{ arcmin}^{-2}$.)

ever there are various difficulties with this idea (Read et al. 1995). Alternatively they could be foreground or background objects, for example quasars or stars, completely unrelated to the diffuse arms. This latter possibility is supported by recent optical observations of source P, the optical feature coincident with the source at the end of the northern streamer, which indicate that it is a distant ($z = 0.155$) galaxy with an active nucleus (L.R.Jones, private communication).

The *Antennae* has also been observed with the *ROSAT* HRI (Fabbiano, Schweizer & Mackie 1996), and the results are generally consistent with the PSPC results. A complex X-ray structure is seen involving filamentary regions, closely following the $H\alpha$ distribution, emission peaks coincident with HII regions, super-Eddington sources, and prominent nuclear sources. There is also some evidence of nuclear outflows and superbubbles.

4.4 NGC 520

The nature of the peculiar system NGC 520 was once a puzzle; is it one disturbed galaxy or two interacting galaxies? Recent studies have clarified the interacting galaxies interpretation. Stanford and Balcells (1990) have detected two galactic nuclei, just visible in the optical but more clearly in their K-band image. The less massive component (by perhaps more than an order of magnitude) is the northwestern knot, which is optically brighter than the main component. The main component is optically weak because it is seen edge-on, and the light from its central region is absorbed by interstellar dust in its disc (visible as a dark lane in Figure 1 of Bernlöhr 1993). Furthermore, Two hypotheses, either that the nearby dwarf galaxy UGC 957 might be primarily responsible for the disturbed morphology of a single galaxy in NGC 520, or that two interacting disc systems formed NGC 520, were tested with numerical simulations (Stanford and Balcells 1991). The simulations indicate that NGC 520

Figure 4. Contours of (0.1–2.3 keV) X-ray emission shown superimposed on an optical image of Arp 4038. Contour levels increase by factors of two from $7.2 \times 10^{-4} \text{ ct s}^{-1} \text{ arcmin}^{-2}$.)

contains two interacting discs which collided $\sim 3 \times 10^8$ years ago and UGC 957 was only involved in the producing of the northern half of a tidal tail.

Tovmasyan and Sramek (1976) found that the compact radio source in NGC 520 is situated in the dark lane between the two visible parts of the system. Condon et al. (1982) later resolved this into a 6'' east-west extension, consistent with an edge-on disc, lying 3° off east-west. Millimeter-wave interferometer maps of the $2.6\mu\text{m}$ CO emission (Sanders et al. 1988a) show a strong peak at the position of this radio source; approximately $1.9 \times 10^9 M_\odot$ of molecular gas is concentrated in a region approximately 0.8 kpc in size.

Much of the extranuclear regions of both galaxies within NGC 520 experienced a period of enhanced star formation $\sim 3 \times 10^8$ years ago. The main sequence remnants of this burst are the A stars whose features are evident in the optical spectra (Stanford 1991). The burst within the less massive (the north-western) nucleus occurred slightly later than in the extranuclear regions, but the star formation rate has returned to a nominal level. The more massive, optically hidden nucleus (to the south-east) produces stars at a rate of $\sim 0.7 M_\odot \text{ yr}^{-1}$ and is the current dominant source of star formation in this system. The star formation rate within this region is ~ 35 times higher than for an isolated disc galaxy. This region dominates the mid-infrared flux of the system, and probably produces most of the far-infrared flux seen in NGC 520. It is still unclear, though, whether the massive star component is sufficient to power the activity at the very centre, even though multi-wavelength observations argue against the presence of a nonstellar compact power source within the south-eastern nucleus (Stanford 1991).

The NGC 520 PSPC data were processed exactly as described in section 3. Figure 5 shows contours of (0.1–2.3) X-ray emission, superimposed on an optical image. Table 6 shows the results of the spectral fitting to the PSPC data as described in Section 3. The one source detected in the vicin-

Source	Spectrum Analysed		Net Counts	$\log L_X$ (0.1–2.0 keV)	Best Spectral Fit Results				
	R.A. (2000.0)	Dec (2000.0)			column 10^{20} cm^{-2}	photon index	temp. keV	Z (solar)	χ^2 (n.d.o.f)
Integrated			2804±61	40.98	$5.50^{+0.50}_{-0.40}$		$0.69^{+0.03}_{-0.03}$	$0.03^{+0.01}_{-0.01}$	23.7 (14)
‘Diffuse’ 1-component fit				40.63	$3.30^{+0.87}_{-0.77}$		$0.49^{+0.07}_{-0.06}$	$0.04^{+0.02}_{-0.02}$	21.56 (14)
‘Diffuse’ 2-component fit			521±32	(RS) 40.61 (Br) 39.51	$3.40^{+0.58}_{-0.00}$ $87.5^{+215}_{-87.5}$		$0.36^{+0.09}_{-0.05}$ 10 (F)	$0.07^{+0.05}_{-0.03}$	17.80 (12)
Source A	12 01 55.4	-18 52 09	475±23	40.28	$8.1^{+1.4}_{-1.1}$		$0.72^{+0.13}_{-0.10}$	$0.00^{+0.01}_{-0.00}$	
Source B	12 01 52.2	-18 52 09	129±12	39.99	$5.1^{+1.6}_{-1.3}$		$0.79^{+0.13}_{-0.13}$	$0.06^{+0.09}_{-0.04}$	
Source C	12 01 50.8	-18 52 20	124±12	39.91	$17.4^{+14.4}_{-7.4}$		$0.68^{+0.26}_{-0.26}$	$0.02^{+0.06}_{-0.02}$	
Source D	12 01 53.3	-18 53 06	520±24	40.16	$13.7^{+5.8}_{-3.4}$		$0.70^{+0.06}_{-0.10}$	$0.10^{+0.07}_{-0.05}$	
Source E	12 01 51.2	-18 53 45	119±12	39.70	$10.5^{+15.8}_{-4.0}$	$2.2^{+1.1}_{-0.5}$			
Source F	12 01 47.9	-18 54 10	53±9	38.98	$1.9^{+5.6}_{-1.9}$		$0.45^{+0.71}_{-0.17}$	$0.02^{+0.64}_{-0.02}$	
Source G	12 01 53.5	-18 51 23	117±13	39.42	$11.5^{+20.4}_{-4.5}$		$0.38^{+0.17}_{-0.15}$	$0.00^{+0.02}_{-0.00}$	
Best ‘Diffuse’ + sources			41.03						

Table 5. The results of the PSPC spectral analysis of NGC 4038/9. Tabulated luminosities are those escaping from the system. Only the best model fit is shown. Errors on the spectral fit parameters are 1σ for one interesting parameter.

Figure 5. Contours of 0.1–2.3 keV X-ray emission from NGC 520 overlaid on an optical image. The contour levels increase by factors of two from $7.2 \times 10^{-4} \text{ ct s}^{-1} \text{ arcmin}^{-2}$.

ity of NGC 520 at $\alpha = 01h24m34.76s$, $\delta = +03d47m39.7s$, lies within $\sim 5''$ of the radio source resolved by Condon et al. (1982), once the residual error of the *ROSAT* attitude solution ($\approx 6''$; Hasinger et al. 1992) is taken into account.

It appears that NGC 520 is a very compact X-ray source with little in the way of diffuse emission. The *Einstein* image (Fabbiano et al. 1992) appears to show the same thing though to a much coarser resolution. This compactness can be seen more clearly in figure 6, a comparison of the radial profile of the emission from NGC 520 (crosses) with the *ROSAT* PSPC PSF (line), where very little emission is seen beyond a radius of 0.6' (the 95% enclosed energy radius of

Figure 6. A comparison of the radial X-ray emission from NGC 520 (crosses) with the *ROSAT* PSPC PSF (line).

the PSPC PSF). The X-ray emission from NGC 520 is almost consistent with point source emission, and what diffuse emission exists, only makes up a very small fraction of the total.

The diffuse emission that could be extracted (using the method described in section 3) amounts to only about 20 counts, and little can be said about its spectral properties, except that it appears soft, perhaps suggestive of a very low-level, cool corona surrounding the system. This apparent lack of diffuse emission in NGC 520 is discussed in detail later in Section 5.2.

The one point source detected, coincident with both the compact radio source resolved by Condon et al. (1982), and with the more massive of the two nuclei, as visible in the K-band image of Stanford & Balcells (1990), appears to dominate the X-ray emission. The power-law fit and the lack

Source Spectrum Analysed			Net Counts	$\log L_X$ erg s $^{-1}$ (0.1–2.0 keV)	Best Spectral Fit Results				
R.A. (2000.0)	Dec (2000.0)	column 10 20 cm $^{-2}$	photon index	temp. keV	Z (solar)	χ^2 (n.d.o.f)			
Integrated		100.2 \pm 10.5	39.94	53.7 $^{+47.7}_{-30.5}$	4.52 $^{+2.83}_{-1.95}$				22.53 (19)
Diffuse		19.4 \pm 10.1	39.12	0.00 $^{+83.1}_{-0.00}$		0.43 $^{+0.21}_{-0.10}$	10.0 $^{+90.0}_{-7.13}$		
Source A	01 24 34.76	+03 47 39.7	84.7 \pm 9.8	39.92	9.27 $^{+11.1}_{-3.86}$	1.90 $^{+0.80}_{-0.56}$			
Diffuse + sources			39.99						

Table 6. The results of the PSPC spectral analysis of NGC 520. Tabulated luminosities are those escaping from the system. Only the best model fit is shown. Errors on the spectral fit parameters are 1σ for one interesting parameter.

R.A. (2000.0)	Dec. (2000.0)	Net counts	$\log L_X$ (erg s $^{-1}$)
H1	01 24 33.51	+03 48 03.5	9.60 \pm 4.5
H2	01 24 34.71	+03 47 41.2	10.3 \pm 4.9
H3	01 24 35.71	+03 47 31.5	9.59 \pm 4.8

Table 7. Sources within NGC 520 detected with the HRI. Luminosities are calculated as described in Section 3.2, using a 0.3 keV (and a 3.0 keV) thermal bremsstrahlung model, corrected for Galactic absorption.

of diffuse emission perhaps point to an AGN as the primary nuclear power source, but NGC 520 is, as shall be seen in Section 5.2, far too X-ray dim. No source is detected at the position of the north-western nucleus, though an elongation of the X-ray contours in this direction is tentatively visible in figure 5.

In contrast to the PSPC image, the HRI image (Fig. 7) shows a great deal of detail. Table 7 gives the positions, net counts and X-ray luminosities (assuming 0.3 keV (and 3.0 keV) bremsstrahlung models) of the detected HRI sources. Three sources are detected, the most northerly, H1, being centred less than 5'' (i.e. less than the residual error in the *ROSAT* attitude solution) east of the secondary (optically brighter) nucleus. This source, undoubtedly associated with the northern nucleus, appears to be the hardest of the sources, as it is the only source detected in the hard band (channels 6–11; see Section 3.2). The suggested extension to the east is interesting, though its existence is tentative. Sources H2 and H3 both appear to be much softer than source H1, and they follow the bright band of optical emission down the north-eastern side of the system. The primary, optically fainter, southern nucleus actually lies slightly south of H2, and west of H3, where some X-ray enhancement is visible.

4.5 Arp 220

Arp 220 (also IC 4553, UGC 9913) is the prototypical ultraluminous galaxy, and is the most luminous object in the local universe. Being the closest and brightest of these IRAS-discovered (Sanders et al. 1988b) systems, it has been extensively studied across the whole range of the electromagnetic

Figure 7. Contours of *ROSAT* HRI X-ray emission from NGC 520 overlayed on an optical image. The contour levels increase by factors of two from 2.2×10^{-3} ct s $^{-1}$ arcmin $^{-2}$.

spectrum. The origin of Arp 220's intense power however, remains still somewhat of a mystery. On the one hand, the huge quantities of dense, warm molecular gas (Scoville & Soifer 1991), together with the strong stellar CO absorption lines observable in the IR (Armus et al. 1995), point to a massive burst of star-formation as the primary energy source. On the other, there appears to be a lot of indirect evidence for the presence of a quasar obscured by a layer of dense gas and dust. Lonsdale et al. (1994), for instance, report a OH megamaser in Arp 220 with an OH line peak originating in a structure \lesssim 1 pc across, and they conclude that most of the emission from Arp 220 arises from a very small region, perhaps on a scale of less than 10 pc, hence the quasar nucleus hypothesis. Prestwich, Joseph & Wright (1994) suggest that, while the IR spectrum of Arp 220 is well fit by a starburst model (Rowan-Robinson & Crawford 1989), its relative deficit of ionizing photons may indicate that it is an evolved starburst, now dominated by an active nucleus. They also point out though, that extinction plus dust absorption of the Ly α photons could result in a much

decreased recombination line flux. A third hypothesis for the production of such large amounts of power, as discussed below, involves the idea of a galaxy-galaxy collision. There is much evidence for Arp 220 being a merger of two galaxies. Majewski et al. 1993, for instance, have observed the very close, double nucleus in the near-IR. The optical morphology is very similar to that seen in dynamical simulations of late-stage mergers of two disc galaxies (e.g. Mihos & Hernquist 1994). Furthermore, Wright et al. (1990), having obtained K-band images of several merging systems, discovered that the radial profile of Arp 220 appeared to follow an $r^{1/4}$ law, typical of elliptical-like, and therefore possibly merger-remnant, systems. Within this merger scenario, it has been suggested (Harwitt et al. 1987), that the FIR emission and the soft X-ray/EUV radiation could be produced by dust heated by the collision, and by the cloud-cloud collisions that occur when two-gas-rich systems encounter one another.

Arp 220 has been observed in X-rays prior to *ROSAT*, with the *Einstein* IPC (Eales & Arnaud 1988). An X-ray sources $\sim 1'$ from the position of Arp 220 was discovered, and was assumed to be associated with the system. Because of the size of the source (thought to be about twice the optical size) and the softness of the spectrum, the authors concluded that the bulk of the emission could not be coming from any obscured active nucleus at the galaxy's centre.

A thorough analysis of both the *ROSAT* PSPC and HRI data from Arp 220 has already been published (Heckman et al. 1996), and a discussion of our results in conjunction with theirs, is presented here. The *ROSAT* image (Fig.8) shows quite clearly why the *Einstein* image was so confusing. Two distinct regions of X-ray emission are seen around Arp 220. One is centred on the system itself, and appears elongated in an approximately east-west direction. The other feature is a large ($\sim 3'$) amorphous structure, and appears to stretch out from Arp 220 to the south and south-west. Two sources are detected. Source A lies within the large southern feature and source B lies at the centre of Arp 220.

The northern feature, the approximately east-west structure centred on source B, at the centre of Arp 220, is large, ≈ 40 kpc long at the distance of 76 Mpc assumed here. Interestingly, Heckman et al.'s (1996) HRI image also shows an elongation (≈ 11 kpc long), though in a more southeast-northwest orientation, misaligned by about 30° with the PSPC feature. The HRI image also shows, at the very centre of the emission, what appears to be a pair of pointlike sources of equal brightness, separated by $\approx 5''$, lying in a southeast-northwest orientation, similar to what is seen in optical R-band and H α images. It seems very likely that this double structure is related to the prominent dust lane running through the centre of the galaxy. The X-ray structure is probably an elongated feature which appears as a double source because of the dust lane running perpendicularly through its centre.

The northern east-west elongated structure appears very similar to the H α emission-line nebula visible around Arp 220 (Heckman, Armus & Miley 1987; 1990), which, as shown by Heckman et al. (1990), appears to be a pair of expanding bubble-like structures. As noted by Heckman et al. (1996), both the X-ray and the optical features show a central maximum, surrounded by a relatively bright, $0.5'$ inner region, elongated in the southeast-northwest direction. Outside this, a larger structure is visible in both the X-ray

and the optical, elongated more in the east-west direction. Heckman et al. (1996) conclude that both the X-ray and the H α features are the same size (to within 10%). They also suggest that both the X-ray and the optical emission arise as the result of a bipolar wind, driven out from the nucleus over a timescale of a few times 10^7 yr by an ultraluminous starburst (though it is also possible that the wind could be driven by a hidden QSO). Heckman et al. (1996) also suggest that the $\sim 30^\circ$ misalignment of the outer structure may reflect a change in orientation of the system, as the encounter has progressed (see Section 5.3.2).

In the previous analyses, the X-ray features seen have not been much larger than the optical sizes of the systems in question (except perhaps in the case of the *Antennae*, where a more rigorous analysis has been performed; see Section 4.3). In Arp 220 however, the X-ray emission extends well beyond the optical confines of the system, and so the spectral extraction procedure has been performed in a different way to that described in Section 3. Firstly, a 'northern' spectrum was formed, in an identical manner to that described in Section 3, from a circular area slightly greater than the optical diameter (actually centred on source B and extending out to a radius of $65''$). Source spectra for sources A and B have been formed exactly as described in Section 3. The 'diffuse' spectrum however, has been extracted from a much larger area, chosen to include the southern emission – a circle of $3'$ radius, centred halfway between sources A and B. The emission from sources A and B has been removed, as described in Section 3.

The 'northern' spectrum and its resultant fits (see Table 8), therefore refer to the whole of the northern feature, the east-west feature surrounding (and including) source B. Heckman et al. (1996), in their fitting of the spectrum obtained from this area, froze the absorbing hydrogen column at two values; the column out of our own galaxy ($3.7 \times 10^{20} \text{ cm}^{-2}$), and the maximum column allowable by the H I data of Baan et al. (1987) ($5 \times 10^{21} \text{ cm}^{-2}$). Neither fit can be excluded. The best fit obtained in our present work (though relatively bad) is consistent with the high-column fit of Heckman et al. (1996). Consequently, our derived $L_X(0.1-2.0 \text{ keV})$ of $1.5 \times 10^{41} \text{ erg s}^{-1}$ is towards the higher side of the Heckman et al. (1996) range. Little can be said about the different spectral components involved in the northern feature except that the central peak (source B), is best fitted with a very high-column plasma, and may be spectrally harder than the total 'northern' emission, indicating that the outer, non-source B emission, - the 'bubble' emission, is likely to be spectrally, quite soft, as is seen in the halos of many starburst and merging systems (e.g. Heckman 1993; Read et al. 1997).

The southern feature is very large, about $3'$ (65 kpc) in diameter, bright, accounting for about half of the total counts, and appears to be spectrally, quite soft - the best fit to the 'diffuse' spectrum (i.e. the entire emission minus the emission from sources A and B) (Table 8) being consistent with a low temperature (6 million K) plasma, absorbed merely by the column within our own galaxy.

Heckman et al. (1996) suggest that this southern feature is associated with a background group/poor cluster of galaxies, though they cannot exclude the possibility that it is in fact, associated with Arp 220. From the apparent magnitudes of the galaxies seen at this position in optical

survey plates, a redshift for the putative group can be estimated, and the implied luminosity, size and temperature of the southern feature turn out to be quite reasonable when compared to known groups or poor clusters. Recent spectroscopic observations of two of these galaxies do show them to have similar redshifts ($z \approx 0.09$; L.R.Jones; private communication) comparable to the values estimated by Heckman et al. (1996). This shows that there is at least a pair of galaxies behind the southern feature, and strengthens the group interpretation.

In order to investigate the spectral characteristics of this southern feature, a ‘southern’ spectrum was extracted from a $1'$ radius circle centred at the position $\alpha = 15^h34^m53.7^s$, $\delta = +23^d28^m32^s$. X-ray emission coincident with the optical galaxies was excluded from the data to avoid possible contamination of the spectrum from sources associated with the galaxies themselves, and then standard spectral models were fitted. The model that best fits this southern spectrum is a Raymond & Smith (1977) hot plasma model with an absorbing column ($5.87 \pm 2.74 \times 10^{20} \text{ cm}^{-2}$) consistent with that out of our Galaxy, a low temperature (0.5 keV), and a very low (< 0.05 solar) metallicity. Further investigation of the temperature-metallicity parameter space however, reveals that the temperature is not very well constrained; the fit is only marginally worse when the temperature is ~ 1 keV, and the metallicity is a few tenths solar. At the distance of Arp 220, the best fit model, once scaled to allow for the flux lost in the removal of emission associated with the background galaxies, gives rise to an emitted (0.1–2.0 keV) X-ray luminosity of $1.4 \times 10^{41} \text{ erg s}^{-1}$. The equivalent luminosity at a distance corresponding to a redshift of 0.09 (360 Mpc) is $2.9 \times 10^{42} \text{ erg s}^{-1}$.

Assuming first that the southern feature *is* associated with Arp 220, the total X-ray (0.1–2.0 keV) luminosity is given by the sum of the luminosities inferred from the spectral fits to each of the ‘southern’ and the ‘northern’ spectra; $\log L_X = 41.47$ (the same figure is reached by the summation of the inferred luminosities of the ‘diffuse’ spectra and sources A and B). If, however, the southern source is *not* associated with Arp 220, then purely the ‘northern’ spectrum gives $\log L_X = 41.18$. The true nature of this feature is discussed later in Section 5.3.

4.6 NGC 2623

NGC 2623 (Arp 243), eighth in the Toomre (1977) sequence of merging systems, exhibits two large-scale, well defined tidal tails, blue colours and distinct regions of star formation (Schombert et al. 1990). Both Toomre (1977) and Joseph and Wright (1985) infer from this morphology that NGC 2623 is the product of a tidal encounter between two similarly massive disc galaxies.

Whereas three distinct condensations can be identified in optical images of NGC 2623’s central region, near-infrared images (e.g. Joy and Harvey 1987, Stanford and Bushouse 1991) reveal a single symmetric nucleus lying between the two northern optical features. Joy and Harvey (1987) conclude that the southern condensation cannot be a remnant nucleus, and may simply be a counterarm generated by the tidal interaction (c.f. Toomre and Toomre 1972). Stanford and Bushouse (1991) find that their K-band surface brightness profile is, as seen in Arp 220, well fitted by an $r^{1/4}$ law,

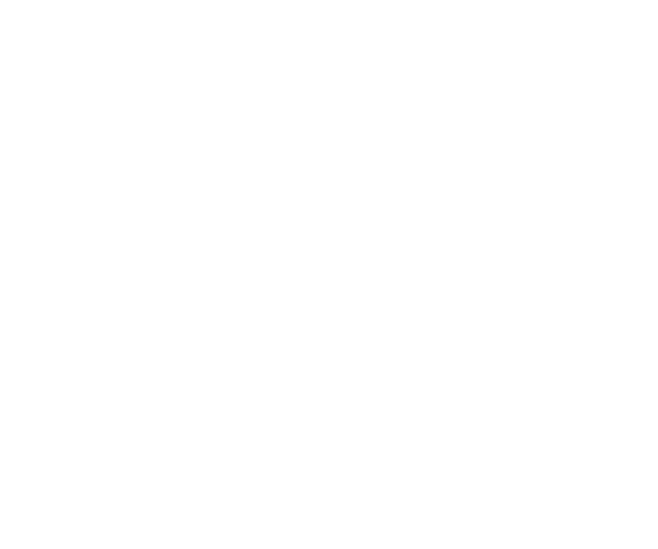


Figure 8. Contours of 0.1–2.3 keV X-ray emission from Arp220 overlayed on an optical image. The contour levels increase by factors of two from $7.2 \times 10^{-4} \text{ ct s}^{-1} \text{ arcmin}^{-2}$.

characteristic of elliptical galaxies, out to 3 kpc. This was also seen by Wright et al. (1990), who concluded that the stellar light profile of NGC 2623 bears a very close resemblance to that of ellipticals.

A radio source in the nucleus of NGC 2623 was resolved at 6 cm (Condon 1980), with a size of 170 pc and a radio spectral index such that $F_\nu \propto \nu^{-0.8}$. The size of the radio source, the slope of the radio continuum, and the ratio of 100 μm to 21 cm flux (Joy and Harvey 1987) are consistent with synchrotron emission from supernovae produced in a burst of star formation (Condon 1980, Condon and Broderick 1986). The radio observations also appear to be consistent with a weak non-thermal emission-line source (c.f. Keel 1986).

Strong Balmer absorption lines reveal the presence of early-type stars in NGC 2623’s nuclear region, making up between one-third to one-half of the central optical emission (Joy and Harvey 1987). Emission lines such as H α and N II, in contrast to the early-type star distribution, are found to originate only within the very centre of NGC 2623, and the high N II/H α ratio observed indicates that the nuclear emission lines are wholly or partially excited by shocks or a weak nonthermal LINER source (Keel 1986). Joy and Harvey (1987) conclude that, since nebular emission lines are not associated with the extended distribution of young early-type stars, most of the highly ionizing O and early B type stars have evolved off the main sequence. A similar conclusion was reached by Larson and Tinsley (1978), who found that NGC 2623 exhibits UVB colours of a galaxy in which a burst of star formation occurred $\approx 10^8$ years ago.

There are several observations indicating that collisions between gas clouds are taking place within NGC 2623. Joy and Harvey (1987), for instance, have inferred that the merger should produce a region of compressed gas and dust $\sim 2''$ in extent. This is observed within the central regions of NGC 2623. Furthermore, observed strong OH absorp-

Source Spectrum Analysed			Net Counts	$\log L_X$ erg s $^{-1}$ (0.1–2.0 keV)	Best Spectral Fit Results				
R.A. (2000.0)	Dec (2000.0)	column 10 20 cm $^{-2}$			photon index	temp. keV	Z (solar)	χ^2 (n.d.o.f)	
'Northern' ^a		168±18.7	41.18	44.0 $^{+19.5}_{-14.4}$		0.21 $^{+0.05}_{-0.04}$	0.00 $^{+0.03}_{-0.00}$	33.8 (18)	
Diffuse ^a		220±33.4	41.37	5.17 $^{+2.46}_{-1.65}$		0.50 $^{+0.13}_{-0.10}$	0.01 $^{+0.02}_{-0.01}$		
Source A	15 34 54.31	+23 28 27.0	49.1±9.5	40.38	24.7 $^{+46.7}_{-24.5}$	3.75 $^{+2.85}_{-1.35}$			
Source B	15 34 56.91	+23 30 10.6	107±12	40.55	63.7 $^{+35.3}_{-25.6}$		0.23 $^{+0.12}_{-0.07}$		
Diffuse + sources			41.47						

Table 8. The results of the PSPC spectral analysis of Arp 220. Tabulated luminosities are those escaping from the system. Only the best model fit is shown. Errors on the spectral fit parameters are 1σ for one interesting parameter.

^a The ‘northern’ and diffuse spectra have been obtained in a different way from that described in Section 3. See text for details.

tion features imply the existence of a dense concentration of molecular clouds in the nuclear region (Baan et al. 1985). Also, CO observations (Sanders et al. 1986, Casoli et al. 1988) indicate that NGC 2623 has $6 \times 10^9 M_\odot$ of molecular hydrogen gas, highly concentrated towards the radio and infrared nucleus, in a region less than 3 kpc in size.

Once the analysis of the system had begun, exactly as described in Section 3, it soon became evident that only a small number of counts were present. The analysis was therefore restricted to the energy band (0.1–1.2 keV), in order to maximise the signal to noise. Figure 9 shows contours of X-ray emission from NGC 2623 not only in the ‘full’ (here, 0.1–1.2 keV) energy band, but also in soft (0.1–0.5 keV) and hard (0.5–1.2 keV) bands. What is very evident from figure 9, is that, as seen in Arp 220, two very distinct components comprise the X-ray emission from NGC 2623; a hard, compact nuclear feature, and a cool feature, lying outside of the optical confines of the system, above the northern edge of the western tail.

Spectral fitting of the integrated, the diffuse and the nuclear feature’s spectra all proved difficult, due to the small number of counts. Only very simple models (thermal bremsstrahlung and power law with the absorbing column frozen at the Galactic value) could be used to fit these spectra (see Table 9), and the maximum likelihood statistic had to be used in every case. Thermal bremsstrahlung models proved the better fit to each spectrum. Although Source A, the nuclear feature, was not actually formally detected at the 4σ significance level, we have included it here on the basis of it having a signal-to-noise ratio greater than 2. Furthermore, because of the low number of counts, we have not given any spectral fitting results regarding source A. Source A’s spectrum does appear to be hard however (as indicated by Figure 9), and a luminosity is given in Table 9, assuming a 1.5 keV bremsstrahlung spectrum absorbed by the column out of our Galaxy.

The X-ray emission from NGC 2623 is split into two very distinct components. The nuclear feature (source A) is compact, and strong, and appears to be spectrally hard. It is coincident with published optical, radio, IR and CO emission. It is also seen with the HRI (see Fig. 10), though only at a very low flux level (3.6×10^{-4} cts s $^{-1}$).

The second feature, lying to the west of the system and coincident with seemingly nothing whatsoever, is of much

Figure 9. Contours of X-ray emission in three different energy bands (top: 0.1–1.2 keV, middle: 0.1–0.5 keV, bottom: 0.5–1.2 keV) are shown superimposed on an optical image of NGC 2623. The contour levels increase by factors of two from 7.2×10^{-4} ct s $^{-1}$ arcmin $^{-2}$.

more interest. Comparison of the radial profile with the PSPC point spread function is inconclusive as to whether the source is extended or not. If the feature is point-like, then the very low temperature could point to a serendipitous quasar or white dwarf as possible candidates. Typical quasar spectra ($\alpha = 2.2 \pm 0.2$; Branduardi-Raymont et al. 1994; Roche et

Source Spectrum Analysed	R.A. (2000.0)	Dec (2000.0)	Net Counts	$\log L_X$ erg s $^{-1}$ (0.1–2.0 keV)	Best Spectral Fit Results				χ^2 (n.d.o.f)
					column 10 20 cm $^{-2}$	photon index	temp. keV	Z (solar)	
Integrated			36.0 \pm 10.3	40.93	3.28(F)		0.49 $^{+0.28}_{-0.22}$		
Diffuse			19.2 \pm 9.4	40.57	3.28(F)		0.20 $^{+0.10}_{-0.08}$		
Source A ^a	08 38 23.54	+25 45 09	9.6 \pm 3.8	40.70	3.28(F)		1.50(F)		
Diffuse + sources				40.94					

Table 9. The results of the PSPC spectral analysis of NGC 2623. Tabulated luminosities are those escaping from the system. Only the best model fit is shown. Errors on the spectral fit parameters are 1σ for one interesting parameter.

^a No spectral analysis results are given for source A due to the low number of counts. The tabulated luminosity assumes a 1.5 keV bremsstrahlung spectrum corrected for Galactic absorption (see text).

al. 1995) however, observed through the Galactic column to NGC 2623, can be shown through simulations, to be far too hard to correspond to this soft component. Furthermore, as only a few hundred white dwarfs were detected in the entire *ROSAT* all-sky survey, it is statistically very unlikely that this feature is due to a foreground white dwarf. It is also very unlikely that the soft feature is associated with the western tail, as it lies well above it, and this tail is both dimmer and less blue than its partner (Schombert et al. 1990). The HRI image (Fig. 10) shows something very interesting however as regards this western feature – nothing at all. Nothing is seen in the HRI data to the west of NGC 2623 on any spatial smoothing scale down to a significance level of 2σ . The lack of any HRI emission is useful, as regards ascertaining whether this feature is point-like or not. If the source were point-like then we should have expected (based on the PSPC count rate) ≈ 0.8 ct ksec $^{-1}$ in the HRI data. This is not seen; a 2σ upper limit to the HRI count rate at the position of the PSPC feature gives 0.2 ct ksec $^{-1}$. Hence, either the western feature is very variable, or it is extended, on a scale substantially larger than the spatial resolution of the HRI. We assume below that the western feature has a maximum extent of $\approx 2'$, as suggested by Figure 9.

The fact that this feature is very soft is reminiscent of the X-ray outflows (or winds) seen around many starburst galaxies (Heckman 1993; Read et al. 1997). If NGC 2623's soft feature is an outflow, then it is a rather different outflow from the standard starburst type; apart from it being far more luminous and cooler, it appears only on one side of the system, and it is a great deal larger (~ 30 kpc).

This large cool, diffuse X-ray structure bears much more resemblance in fact, to the feature seen in the previous section; the large amorphous structure to the south of Arp 220, a system very similar to NGC 2623 (hence their adjacent positions in the present sequence), with comparable IR luminosities, and similar elliptical-like light profiles (Wright et al. 1990). The feature in Arp 220, as discussed in the previous section, is believed by Heckman et al. (1996) to be associated with a galaxy group or small cluster. In the case of NGC 2623, however, nothing is seen in the optical. The nature of these features is discussed later in Section 5.3.

Figure 10. Contours of *ROSAT* HRI X-ray emission from NGC 2623 overlayed on an optical image. The contour levels increase by factors of two from 2.2×10^{-3} ct s $^{-1}$ arcmin $^{-2}$.

4.7 NGC 7252

In Toomre's (1977) sequence of merging systems, NGC 7252 (Arp 226) appears last, its structure, combining a single relaxed-looking body with long, faint tidal tails, suggestive of a possible end-product of the merger process – an elliptical galaxy. Schweizer (1978) found many features within this galaxy, often compared to the 'atoms for peace' symbol, which conclusively defined NGC 7252 as a late-stage merger. These features included two similar, oppositely-moving tidal tails, a single relaxed nucleus, chaotic motions within the main body, ripples and loops at the edges of the main body, and no nearby perturbing systems. Further work showed that the light from NGC 7252 follows an $r^{1/4}$ law (e.g. Stanford & Bushouse 1991), typical of ellipticals, it exhibits a post-starburst nuclear population (Schweizer 1982), and it obeys the Faber-Jackson relationship (Lake & Dressler 1986), again characteristic of normal elliptical galaxies. Many more recent studies have strengthened the

idea that NGC 7252 is a late-stage merger of two gas-rich spiral discs (e.g. Schweizer 1990; Hibbard et al. 1994), and it is now considered to be the prototype merging galaxy remnant. Perhaps the strongest observational support of the merger hypothesis comes from the recent VLA observations of NGC 7252 (Hibbard et al. 1994), where, while the tidal tails were seen to be very abundant ($2 \times 10^9 h^{-2} M_\odot$) in atomic hydrogen, a fact requiring a gas-rich spiral genesis, the main body of the system was seen to be virtually empty of H I, and appears indistinguishable from a typical elliptical. The molecular gas, in contrast to the atomic gas, is tightly bound to an inner rotating disc, of radius $\approx 7''$, the gap between the atomic and molecular gas distributions apparently filled by diffuse H α emission. The H I within the tidal tails of NGC 7252 is very interesting: the M_{H_1}/L_B ratio is consistent with that seen in the outer regions of late-type spirals (~ 1 ; Wevers et al. 1986), and the gas and starlight in the eastern tail appear to have the same extent, whereas in the northwestern tail, the neutral hydrogen appears to extend some 40 kpc or so beyond the optical emission. From the work of Cayatte et al. (1994), this may indicate that the progenitor galaxy that gave rise to the eastern tail may be of an earlier type than its partner (Hibbard et al. 1994).

Computer simulations of collisions between two gas-rich discs (Borne & Richstone 1991; Mihos et al. 1993) reproduced the essential features of NGC 7252's appearance at first, quite adequately, though a retrograde encounter geometry (i.e. galaxy rotations in the opposite sense to their mutual orbit), and a very tightly bound orbit, such that the galaxies were in contact at the start of the simulation, were necessary. These simulations were later however, found to be inconsistent with the H I data of Hibbard et al. (1994), and only the more recent simulations of Hibbard & Mihos (1995) are able to match the observations (and with a much more astrophysically satisfying orbital geometry), explaining the H I in terms of the material within NGC 7252's tails, having reached a turning point in its expansion, falling back to smaller radii. It is thought that approximately half of the present tail material ($\approx 10^9 M_\odot$ of H I, and $2 \times 10^9 L_\odot$ of starlight) will return to the main body over a timescale of less than 1 Gyr.

NGC 7252 has never been observed in X-rays previously, and the *ROSAT* PSPC and HRI observations presented here, give us a first glimpse at this important system in X-rays. A brief analysis of the PSPC data has already been published in Hibbard et al. (1994), and their X-ray image appears very similar to our Figure 11, though we have contoured the present image to a greater depth. The X-ray source coincident with NGC 7252 appears very centrally concentrated and compact, though a couple of tentative extended features are seen, apparently connected to the main body, to the east and to the northeast. A comparison of the PSPC PSF with a radial profile of the X-ray data centred on the peak of the emission, suggests that the source is resolved, though only at the 2σ significance level.

The best fit to the integrated spectrum indicates that the emission from NGC 7252 may be due mainly to quite cool (0.43 keV) gas. As discussed in the last paragraph, the emission from NGC 7252 may only just be resolved, and consequently, the source-subtraction procedure described in Section 3 had great difficulties in splitting up this emission into source and diffuse emission. In fact, only when a very

Figure 11. Contours of 0.1–2.3 keV X-ray emission from NGC 7252 overlayed on an optical image. The contour levels increase by factors of two from $7.2 \times 10^{-4} \text{ ct s}^{-1} \text{ arcmin}^{-2}$.

large radius ($4'$) was used, could the fitting of the diffuse spectrum settle at sensible values. As can be seen from Figure 11 however, the use of such a large extraction radius merely results in the inclusion of emission from features having nothing to do with NGC 7252, notably from features along the left-hand edge of Figure 11 (see Section 5.5).

Consequently, we have assumed the integrated spectral fit results to be the best indicator of the true (0.1–2.0 keV) X-ray luminosity; $5.3 \times 10^{40} \text{ erg s}^{-1}$. The spectrum is best fitted by a low temperature plasma, indicative of hot gas enveloping the system (the fact that the fitted absorbing column appears larger than the Galactic value probably indicates some contribution from harder, unresolved sources, embedded deeper within the galaxy).

A number of these sources in fact appear in the HRI image (Figure 12), where a great deal of structure is seen. Two sources are formally detected close to the central body of the system (see Table 11). Source H1 is bright, and appears to be coincident with the nucleus, lying less than $7''$ from the position given in the RC3. Features are also seen almost symmetrically opposed to the southeast and northwest of the nucleus. Source H2 is especially interesting, as firstly, it appears to be coincident with the base of the eastern extension tentatively seen in the PSPC image (Figure 11), and secondly, it is the only significant feature detected in the hard band. Interestingly, the northeastern feature seen in the PSPC image appears also to have a tentative counterpart visible in the HRI image (to the top-left of Figure 12).

4.8 AM 1146-270

AM1146-270 was selected from the Arp-Madore *Catalogue of Southern Peculiar Galaxies and Associations* (Arp and Madore 1987). It has a very complex knotty structure within its central $10''$, as indicated by the B-band image of Smith and Hintzen (1991), where seven local maxima, none of

Source	Spectrum Analysed		Net Counts	$\log L_X$ erg s ⁻¹ (0.1–2.0 keV)	Best Spectral Fit Results				χ^2 (n.d.o.f)
	R.A. (2000.0)	Dec (2000.0)			column 10 ²⁰ cm ⁻²	photon index	temp. keV	Z (solar)	
Integrated			225±17.2	40.73	5.20 ^{+2.68} -2.68		0.43 ^{+0.21} -0.21		17.6 (19)
Diffuse ^a			142±46.2	40.39	0.00 ^{+1.83} -0.00		0.09 ^{+0.05} -0.09	0.00 ^{+0.32} -0.00	
Source A	22 20 44.54	-24 40 43.9	165±14.3	40.65	6.09 ^{+1.79} -1.39		0.49 ^{+0.14} -0.10		
Diffuse + sources				40.84					

Table 10. The results of the PSPC spectral analysis of NGC 7252. Tabulated luminosities are those escaping from the system. Only the best model fit is shown. Errors on the spectral fit parameters are 1σ for one interesting parameter.

^a The diffuse spectrum has been obtained in a different way from that described in Section 3. See text for details.

AM1146-270 received only 601 seconds of PSPC time. No significant emission was detected from this system, so a 2σ upper limit to the count rate was derived at the position given in Smith and Hintzen (1991); 4.47 ct ksec⁻¹. Assuming a 1 keV bremsstrahlung plasma and Galactic absorption (5.18×10^{20} cm⁻²) then an upper limit to its emitted (0.1–2.0 keV) X-ray luminosity can be derived; $L_X < 3.9 \times 10^{39}$ erg s⁻¹ (the equivalent 5 keV bremsstrahlung upper limit is 4.1×10^{39} erg s⁻¹).

Figure 12. Contours of *ROSAT* HRI X-ray emission from NGC 7252 overlayed on an optical image. The contour levels increase by factors of two from 2.2×10^{-3} ct s⁻¹ arcmin⁻².

	R.A. (2000.0)	Dec. (2000.0)	Net counts	$\log L_X$ (erg s ⁻¹)
H1	22 20 44.56	-24 40 36.4	19.9±5.3	40.83 (40.67)
H2	22 20 46.56	-24 40 49.2	6.82±3.1	40.36 (40.21)

Table 11. Sources within NGC 7252 detected with the HRI. Luminosities are calculated as described in Section 3.2, using a 0.3 keV (and a 3.0 keV) thermal bremsstrahlung model, corrected for Galactic absorption.

which seem to be superimposed stars, are seen. A plume or fan (13'' in length) extends from the western side of the galaxy (see Fig. 1). The colours are very blue, similar to those of an irregular galaxy, and many blue knots are seen surrounding the nucleus (Smith and Hintzen 1991). This galaxy was detected by IRAS and appears to be the site of much recent star formation.

5 DISCUSSION – THE X-RAY EVOLUTION OF MERGING GALAXIES

The previous subsections have described the X-ray properties of eight systems thought to be at different evolutionary stages of a merger of two disc galaxies. These systems range from ‘approaching’ mergers, such as Arp 270, and Arp 242, where the discs of the two galaxies are still quite distinct, and bridges and tails have only just begun to form, through to ‘contact’ mergers, such as the *Antennae* and NGC 520, where, though the galactic nuclei are still quite distinct, the galactic discs have begun to interact strongly, through to ‘ultraluminous’ mergers, such as Arp 220 and NGC 2623, extremely powerful systems on the point of nuclear coalescence, and finally, to ‘remnant’ mergers, such as NGC 7252 and AM 1146-270, relaxed, elliptical-like systems, their violent star-formation episodes long-since over.

Although we are assuming here that these eight systems represent an evolutionary sequence, one must be careful not to assume that they represent eight different evolutionary stages of the same system, for several reasons. Firstly, the progenitor galaxies are/were all different in detail, in terms of masses, mass ratios, gas richness etc. Secondly, the process by which each system has come about, i.e. the encounter geometries and parameters, will have all been different. Both of these facts are bound to affect the evolution of the system. The fact however, that we have used the appearance, length and symmetry of each system’s tidal tails as one of our main selection criteria, means that we are likely to have selected broadly similar systems, i.e. prograde, medium impact parameter, collisions of similarly-sized disc galaxies. Forces need to act for a long time for the formation of strong tails, and this requires a predominantly prograde encounter (Toomre & Toomre 1972). Similarly, the force needs to be

strong, i.e. the impact parameter needs to be small (Barnes 1992), though not so small as to cause the galaxies to merge before the tails have had a chance to grow. Lastly, proper, symmetrical tail construction requires that the two masses should be roughly equal (Toomre & Toomre 1972).

Therefore, we should really think of the following evolutionary discussion in conservative terms, not as snapshots of a single system at different points in its evolution, more in general terms of how systems appear compared to one another, at ‘approaching’, ‘contact’, ‘ultraluminous’, and ‘remnant’ stages.

5.1 Previous related work

Before continuing, it is useful to review here more fully relevant work on the evolution of interacting systems in other wavebands.

Joseph & Wright (1985) studied the infrared properties of a sample of merely intermediate-age mergers (i.e. covering a smaller evolutionary period than in the present study) including three of the systems within our sample, namely NGC 520, NGC 2623, and Arp 220. None of the systems covered either showed two distinct discs, as in the ‘nearby’ mergers, or appeared as relaxed or elliptical-like as NGC 7252. Nevertheless, their results are of great importance; they observed the infrared luminosity to rise and fall along their sequence, suggesting that a massive burst of star-formation of luminosity $\sim 10^{12} L_\odot$ occurs within merging galaxies as the merger progresses.

Telesco et al. (1988) studied a large sample of comparable-sized interacting galaxies from the Arp-Madore *Catalogue of Southern Peculiar Galaxies and Associations* (Arp and Madore 1987). They found that the dust colour temperature and the interaction strength are both at their largest for systems with the smallest galactic separations. This result, along with those of Joseph & Wright (1985) above, have, as discussed in Section 2, been used in our selection and chronological ordering criteria (see Table 1).

More recently, perhaps the most important work concerning the evolution of merging galaxies has been the work of Hibbard & van Gorkom (1996), and it is worth summarising some of their more important results here, as many of them will have a substantial bearing on the discussion of the X-ray results in the next section.

Hibbard & van Gorkom (1996) presented aperture synthesis observations of the neutral hydrogen distribution in a sample of five systems (four of which are taken from the Toomre (1977) sequence, and three of which (Arp 242, NGC 520 and NGC 7252) appear here). This they supplemented with wide field, narrow band $H\alpha$ images and deep R-band surface photometry.

They found that, within the inner regions, the starlight in the later systems (including NGC 7252) exhibited $r^{1/4}$ profiles, a natural consequence of violent relaxation (Lynden-Bell 1967; van Albada 1982), and obeyed the Faber-Jackson relationship, indicating that as these later systems can be dated at about 1 Gyr after the merger (Schweizer 1996), the primary characteristics of ellipticals are created rather rapidly compared to the total merging time-scales.

The ionized hydrogen is seen, in the early systems (including Arp 242), to form minor axis plumes, similar to the wind ‘blow-outs’ of Heckman et al. (1993), and in the later

systems, to be confined to the inner kpc, presumably associated with a small molecular gas disc.

The cold gas is especially interesting, and is seen to be widely separated in the later systems, with the molecular gas concentrated within the remnant bodies and the atomic gas predominantly in the outer regions. Simulations have shown that the symmetric forces experienced during a merger can force at most half of the outer disc material into a tail, the rest of the $H\alpha$ being forced into the inner regions (Hibbard & Mihos 1995). As less than a quarter of the total $H\alpha$ is found within these regions however, Hibbard & van Gorkom (1966) concluded that most of the centrally forced gas must have been converted during the merger to some other form.

One possibility for what has happened to this gas, is that it has been turned into stars, and indeed, the presence of an ‘E+A’ spectrum (Dressler & Gunn 1983) in NGC 7252 (Fritze-von Alvensleben & Gerhard 1994), and in the almost identical NGC 3921 (Schweizer 1996), indicates that a significant amount of the original atomic gas has formed stars. Another possibility for the fate of the atomic gas, is that it has been converted into molecular gas, though the fact that both NGC 7252 and NGC 3921 have below average molecular gas contents for their spiral progenitors (Solomon & Sage 1988; Young & Knezec 1989), indicates that there has been little net conversion of atomic to molecular gas. A third possibility for the lost atomic gas, is that it has been heated to X-ray temperatures, either through cloud-cloud collisions (Harwitt et al. 1987), or through the energy input from massive stars and supernovae created in one (or, as discussed later, more than one) starburst(s). This neatly brings us on to the X-ray evolution.

5.2 The X-ray evolution

In Table 12 we have gathered together the emitted 0.1–2.0 keV X-ray luminosities of the eight sample systems, calculated as explained in Sections 4.1 to 4.8. Note that in the case of Arp 220, we have given the X-ray luminosity of only the northern feature, the southern outflow/group emission has been omitted (inclusion of this emission raises L_X to 2.9×10^{41} erg s⁻¹ – see Section 4.5).

Also shown in Table 12, are the statistical errors (expressed as percentages), based on the number of counts (including background), for each source. There is, in addition to this statistical error, a second error which arises from uncertainty in the appropriate model to use. Since the X-ray luminosities derived here are band limited to the 0.1–2.0 keV band, the effects of considering different acceptable models are not very large. Comparing the luminosities inferred from power-law and hot plasma models in cases where these give fits of comparable quality, we find differences of ~ 1 –15% (the larger variations applying to the lowest count-rate cases). For a given spectral model, the effects of varying the model parameters within the 90% confidence contour results in luminosity variations of the same order. As can be seen from Table 12, these uncertainties in L_X are similar in size to the simple statistical flux errors.

In order to see how these X-ray luminosities compare with the various multiwavelength properties given in Table 1, what is needed is a plot of the various different luminosity ratios (L_X/L_B , L_X/L_{FIR} etc.) as a function of merger age. As discussed earlier, even establishing a reli-

System	Other names	$\log L_X$ (erg s^{-1}) (% error)
Arp 270	NGC 3395/6	40.49 ^a (10.3 %)
Arp 242	NGC 4676	40.76 ^b (35.3 %)
NGC 4038/9	Arp 244	41.03 ^{a,c} (2.6 %)
NGC 520	Arp 157	39.94 ^b (9.5 %)
Arp 220	UGC 9913	41.18 ^{b,d} (11.1 %)
NGC 2623	Arp 243	40.93 ^b (28.6 %)
NGC 7252	Arp 226	40.67 ^b (7.6 %)
AM 1146-270		<39.61 ^e (-)

Table 12. The merging galaxy sample. Emitted (0.1–2.0 keV) X-ray luminosities have been calculated as described in Sections 4.1 to 4.8, by using the spectral fits to various spectra, as follows (quoted errors are purely statistical; see text):

^a Summation of the best 2-component fit to the diffuse spectrum plus fits to individual source spectra

^b Best fit to the integrated spectrum.

^c See Read et al. (1995).

^d Note for Arp 220, the ‘northern’ spectrum has been used, i.e. emission from the southern component has been ignored (inclusion of this component increases L_X to $2.9 \times 10^{41} \text{ erg s}^{-1}$).

^e 2σ upper limit (using a 5 keV bremsstrahlung model).

able chronological ordering is fraught with difficulties, and dynamical ages for these systems are considerably more uncertain. However, we are interested in broad trends through the merger process, rather than precise timescales.

With this in mind, Fig. 13 shows the temporal variation of the X-ray, the far-infrared, the optical and the radio luminosities for the merging galaxy sample. Also plotted is the variation of the far-infrared colour temperature, S_{60}/S_{100} . All values have been scaled to those of the first system in the sequence, Arp 270. Shown for comparison, again scaled to the values of Arp 270, are, to the left, the mean values of $LFIR/L_B$, L_X/L_B and L_X/L_{FIR} of both the starburst and normal spiral galaxy samples from Read et al. (1997), and to the right, the sample of elliptical and S0 galaxies from Mackie & Fabbiano (1997). When compared to the results of Fabbiano et al. (1992), we find that the X-ray luminosities of both NGC 7252 and AM 1146-270 (upper limit) are very low when compared to typical ellipticals. It should be noted however, that L_X/L_B for ellipticals is very L_B -dependent, and so, the ‘remnant stage’ galaxies’ X-ray properties should really be compared with those of elliptical galaxies of similar optical luminosity. It is seen though, that the X-ray luminosity of NGC 7252 does appear to be quite low when compared to similarly optically bright systems (again from Fabbiano et al. 1992), and although only an upper limit to the X-ray luminosity from AM 1146-270 could be established, this limit is still quite restrictive, and its X-ray luminosity also appears to be quite low when compared to systems with a similar (very low) optical luminosity (note that very few systems appear in this region of $L_X - L_B$ parameter space in Fabbiano et al. (1992), so this result is not very secure).

The interaction timescales in Fig. 13 are certainly only approximate, though in the establishing the evolutionary positioning, we have been able to use a variety of pointers. Firstly, for convenience, we have placed time zero at the point of nuclear coalescence, chosen here to be at

the position of the brightest system Arp 220. Now, it is thought from its tail kinematics and spectral properties (Fritze-v. Alvensleben & Gerhard 1994; Schweizer 1990) that NGC 7252 is at ~ 1 Gyr after nuclear merger – hence its positioning. AM 1146-270’s colours and morphology suggest that it is somewhat older. On the younger side of the evolution, comparison of the general morphologies of the sample galaxies with the numerical simulations of Mihos & Hernquist (1996) suggest ~ 650 Myr between an Arp 270-type system and nuclear coalescence. Finally, NGC 520, whose simulation lookalikes seem to occur over halfway in, is thought to have experienced extranuclear starburst activity, as is ongoing in the *Antennae*, and perhaps the *Mice*, some 300 Myr ago (Stanford 1991).

The evolution appears to start, as one would perhaps expect, at an activity level somewhere between that of normal and starburst spiral galaxies. The level of activity, whether given by $LFIR/L_B$, L_X/L_B , $LRAD/L_B$ or S_{60}/S_{100} , rises during the evolution, to well in excess of that of typical starburst galaxies, and then falls again, back to a very similar level to that at the start. Bearing in mind that elliptical galaxies may well be the end-products of this evolution, it is interesting to note that the final L_X/L_B level is quite low when compared to that of typical ellipticals, though it is within the accepted activity range. Interestingly, there is some evidence that the continued evolution of L_X/L_B of even later merger remnants (i.e. moving further to the right) is seen to rise gradually to a level in line with that of typical ellipticals (Mackie & Fabbiano 1997). The X-ray properties of these merger remnants are discussed in more detail in Section 5.4.

What may be of critical importance is a comparison of the far-infrared evolution (which we may assume bears a very close resemblance to the evolution of the current star-formation rate, SFR) with the theoretical work of Mihos & Hernquist (1996). These authors used numerical simulations to investigate the gas dynamics and starbursts in mergers similar to those considered here (i.e. of systems of comparable mass). They found that the actual structure of the galaxies plays a dominant role in the evolution of the SFR. Two merging scenarios, identical except for the make-up of the systems, were considered. One consisted of a merger of pure disc/halo systems, systems completely lacking a bulge component, the other consisted of a merger of disc/bulge/halo systems, each dense bulge component having a mass some three times that of the disc component. It was found that the gaseous inflows (which are related to the SFR, and hence to the FIR luminosity) are strongest when galaxies with dense central bulges are in the final stages of merging.

Firstly, let us discuss the SFR evolution of the non-bulge mergers. The SFR in these systems is seen to peak at 40–60 times field spiral values at a time some 500 Myr before nuclear coalescence, this peak lasting for about 150 Myr, i.e. from a time around the position of Arp 242, till soon after the position of the *Antennae*. As these starbursts deplete the nuclear regions of gas, the starbursts die out, and the SFR is seen to drop again close to its quiescent value at about the position of NGC 520. During nuclear coalescence (at time zero), only a relatively weak starburst is produced (an increase in the SFR by about an order of magnitude, and lasting for around 50–100 Myr). The SFR history of the bulge mergers however, is very different and bears a very close

Figure 13. The evolution of the merging galaxy sample. Plotted is the temporal variation of the X-ray, the far-infrared, the optical and the radio luminosities for the merging galaxy sample. Also shown is the variation of the far-infrared colour temperature, S_{60}/S_{100} . All values have been scaled to those of the first system in the sequence, Arp 270. Also shown for comparison, are, to the left, the mean values of $LFIR/L_B$, L_X/L_B and $L_X/LFIR$ of both the starburst (stars) and normal (diamonds) spiral galaxy samples of Read et al. (1997), and to the right, the Mackie & Fabbiano (1997) elliptical and S0 sample.

resemblance to Fig. 13. The starbursts that develop after the initial encounter are much weaker than those seen in the bulgeless case. The SFR is increased by only a factor of a few (less than an order of magnitude), though, as the gas is not significantly depleted, it lasts longer, from about Arp 270, or just after, to just before Arp 220. Consequently, at close to time zero, far more gas exists, and the rapid collapse of this gas leads to a very violent starburst, with an SFR some 150 times that of a field spiral, lasting for only 50 Myr. In both the bulge and the non-bulge cases, continued infall of the tidal debris is unable to fuel any significant star-formation, and the remnant after nuclear merger evolves passively at a SFR level similar to that of field spirals.

In reality, galaxies may have a wide range of bulge-to-disc ratios, and mergers occur between galaxies of all types. Although our merging sample has not been chosen with a constant bulge-disc ratio in mind, all the systems seem to show the signature of high-bulge progenitors, when compared to Mihos & Hernquist's (1996) work. The early sys-

tems (Arp 270, Arp 242 and the *Antennae*) show only modest increases in $LFIR$, perhaps by a factor of ten, above normal field spirals. Similarly, the 'ultraluminous' systems' progenitor galaxies must have had large bulge-to-disc ratios, because of their massive inferred SFRs. This does throw up further caveats regarding the difficulty of an evolutionary analysis. Firstly a disturbed morphology does not necessarily mean that a very large burst of star-formation is taking place, and secondly, the main requirements for the existence of an ultraluminous starburst may be specific encounter geometries and/or specific galaxy structures (Hibbard & van Gorkom 1996).

Comparing the X-ray and far-infrared evolution, one sees that although both rise and fall along the merger sequence, the X-ray does so to nowhere near the extent of the far-infrared (and, to a lesser extent, the radio). This leads to the drop by well over an order of magnitude in $L_X/LFIR$ in Fig 13. Before concentrating on this important feature of the evolution however, the striking 'glitch' in the L_X/L_B

evolution associated with the system NGC 520, should first be discussed.

NGC 520, the ‘second brightest very disturbed galaxy in the sky’ (Arp 1987), while once thought, as discussed in Section 4.4, to be a single exploding galaxy (e.g. Arp 1967), is now believed, after receiving so much attention over the years, to be a merger-induced system (e.g. Stanford & Balcells 1990, 1991; Bernlöhr 1993). Its far-infrared properties, as seen in Fig. 13, appear to sit nicely on the evolutionary sequence. Its X-ray properties however, do not. NGC 520 is very underluminous in the X-ray, with an L_X/L_B ratio similar to that of normal (i.e. non-starburst) field spirals. Note that NGC 520’s very low L_X/L_{FIR} ratio (similar to that of Arp 220 and NGC 2623) is very unlikely to be due to the same phenomenon as in the cases of these ultraluminous mergers, as they have *high* L_X/L_B ratios, NGC 520 does not. It is, quite simply, X-ray dim.

This can be seen very clearly in Fig. 14, where the X-ray and far-infrared luminosities of the eight merging galaxies are plotted (AM 1146-270’s upper limit as an arrow), together, for comparison, with Read et al.’s (1997) samples of normal and starburst spiral galaxies. Best fit regression lines (excluding the AM 1146-270 upper limit) to the merging galaxy sample data are plotted both inclusive and exclusive of NGC 520. Also plotted is the best fit regression line to the Read et al. (1997) sample.

NGC 520 stands out quite obviously in Fig. 14. Although very far-infrared bright, as bright as the brightest non-interacting starbursts, it is X-ray underluminous by nearly an order of magnitude. Why? There is quite a lot of evidence to suggest that NGC 520 is a quite different system from the rest of this merging sample.

A strange feature of NGC 520 is the fact that the disc is still remarkably intact; a rotating disc of neutral hydrogen of mass a few $\times 10^9 M_\odot$ and radius ~ 20 kpc is seen within the centre of NGC 520 (Hibbard & van Gorkom 1996). Optical isophotes indicate that both nuclei are embedded within this disc. The disc has survived the merger so far very well. What is to say it that it will not survive the nuclear coalescence? Why NGC 520’s disc has survived so well is somewhat of a mystery, though numerical simulations (e.g. Quinn et al. 1993) suggest that the mass ratio may be very important. For dynamically cold discs to be significantly disturbed, violently fluctuating fields such as those accompanying moderate mass-ratio interactions ($M_1/M_2 > 0.3$) are required. For NGC 520, whilst molecular linewidth studies (Sanders et al. 1988a) and stellar velocity dispersion measurements (Stanford & Balcells 1990) suggest mass ratios close to unity, rotation curves (Bernlöhr 1993) give a mass ratio of 10:1.

While the presence of a large gaseous disc within the merging system requires at least one of the progenitors to have been gas rich, Hibbard & van Gorkom (1996) observe the extensive plumes within NGC 520 to be gas-poor ($M_{H_2}/L_R \lesssim 0.1$), suggesting that NGC 520 came about through the merger of gas-poor progenitor discs (S0–Sa galaxies). The most likely scenario offered by Hibbard & van Gorkom is that the NGC 520 system is a result of an encounter between a gas-rich system with an extensive disc and a gas-poor system, such as an S0 or Sa galaxy. They also conclude though that NGC 520 shows strong evidence that mergers may not necessarily destroy the gaseous discs of the progenitors and therefore need not evolve into ellipticals.

Another related possibility, given that extensive-disc (i.e. near-bulgeless) systems may be involved, is that NGC 520 may be the result of a merger between two bulgeless systems, i.e. as in the evolution of Mihos & Hernquist (1996) discussed earlier, though its relatively low SFR would mean that it must be at an evolutionary stage sometime after the early strong starburst seen in these simulations. Either way, because of the different encounter progenitors involved, whether in terms of mass ratio, gas richness or bulge-to-disc ratio, NGC 520 does appear to be on a significantly different evolutionary path to the rest of the sample.

Turning now to the X-ray evolution of the sample as a whole, it is worth studying Fig. 13 and Fig. 14 together. A rather tight $L_X:L_{FIR}$ relationship is seen in Fig. 14, running quite smoothly and continuously from quiescent normal spirals (diamonds), through starbursts (stars) to very active merging galaxies (filled squares). There does appear however, to be a gradual flattening of the slope at higher activities, and this is borne out by the large change in the slopes of the regression fits, from 0.80, for normal spirals, to 0.38 (0.31 when NGC 520 is discounted) for the merger sample.

Why does this flattening of the $L_X:L_{FIR}$ relationship occur? Also, why does the large drop in the X-ray to far-infrared luminosity ratio, seen in Fig. 13, occur? We believe the answer to both questions to be the same, as both the $L_X:L_{FIR}$ flattening, and the L_X/L_{FIR} drop are really just the same effect manifesting itself in two different ways. As the merger progresses, starburst activity is seen to rise and fall. The increases in both the far-infrared and the X-ray luminosity are both due to the increased starburst activity. While the infrared flux is primarily due to dust heated by the massive stars within the starburst, the rise in X-ray flux is limited, as much of the input energy from the large number of supernovae and stellar winds created within the starburst, is lost. It is most likely that this energy is lost in the form of kinetic energy – kinetic energy associated with the huge gaseous ejections seen in the X-ray in the most luminous members of the merging galaxy sample. We now move on to discuss these diffuse structures.

5.3 Diffuse structures

Diffuse structures, as described in the notes on the individual systems, are observed throughout almost the whole of the evolutionary sequence. Arp 270’s two point sources appear to be embedded in a small amount of diffuse emission, though this emission does not seem to extend very far (if at all) beyond the optical confines of the system. The two sources are both best-fitted by warm plasma models, however, suggestive of hot gas. Arp 242’s distance makes it hard to make any firm judgements about the extent of any diffuse structures. The fact that the source appears extended however, along with the fact that the emission is significantly softer than in Arp 270, is very suggestive of significant amounts of hot gas. Furthermore vigorous disc-wide star-formation is seen in H α within this system, along with plumes of gas extending along the minor axis, possibly coincident with the north-west X-ray feature. The coincidence of H α and X-ray features extending along the minor axis of this system points towards the existence of a galactic wind or ‘blowout’ (e.g. Heckman 1993), NGC 4038/9, as discussed

Figure 14. Plot showing the *ROSAT* (0.1–2.0 keV) X-ray luminosity versus far-infrared luminosity, L_{FIR} , calculated as described in Section 2, for all members of the merging galaxy sample (filled squares) (AM 1146-270's upper limit is shown by the arrow). Also shown, for comparison, are the results for the samples of normal (diamonds) and starburst (stars) spiral galaxies from Read et al. (1997). Best fit regression lines (excluding the AM 1146-270 upper limit) to the merging galaxy sample data are plotted both inclusive (dashed line) and exclusive (solid line) of NGC 520. Also plotted is the best fit regression line to the Read et al. (1997) sample.

briefly here, and in detail in Read et al. (1995), shows a great deal ($\sim 10^9 M_{\odot}$) of low temperature (0.4 keV) gas, not only enveloping the two discs, in what appears to be a hot corona, but also apparently ejected from the system to the north and south as a pair of galactic winds. NGC 520 is very compact, and shows little evidence for any significant amount of diffuse gas. However, as we have already discussed, this system may well be an oddity. Arp 220, the most active of the sample, shows a 40 kpc long, east-west structure, coincident with a ‘double-bubble’ $H\alpha$ emission-line nebula (Heckman, Armus & Miley 1987; 1990). This X-ray/optical emission is generally believed to be due to a bipolar wind driven out from the nucleus by an ultrapowerful starburst. The large soft source to the south of the galaxy is apparently connected to Arp 220, though it may in fact be associated instead with a background galaxy group, as discussed in Section 4.5. However, NGC 2623, a very similar system to Arp 220, exhibits a near-identical feature, which seems a remarkable coincidence. NGC 2623’s very soft (~ 0.2 keV) feature appears to be truly diffuse, given that it is not seen with the HRI. NGC 7252, a near elliptical-like remnant, shows some evidence for an X-ray halo. This halo of hot gas surrounding NGC 7252, however, appears small. And finally, only an upper limit could be calculated for AM 1146-270, due to the very short observing time. It is however, quite a restrictive limit, and places the activity level of AM 1146-270 close to that of NGC 7252, and definitely far less than that of the ultraluminous systems.

The time evolution of the temperature, the size, and the $L_X(\text{diff})/L_B$ values of these diffuse structures are summarized in Fig. 15. All values have been scaled to those of the *Antennae* since Arp 270’s diffuse emission is only suggestive. Two sets of points are plotted for Arp 220, one (the higher set) for the case where the southern source is assumed to be

associated with Arp 220, and the other (the lower set), for the case where it is not. In a discussion of the trends seen within this figure, one must be very conservative. The extraction of truly diffuse emission and the fitting of models to these spectra has been, as described earlier, difficult. Even so, there is evidence that, as a merger progresses, hot gas is ejected from the system. This gas is seen to grow both in size and in X-ray brightness. Curiously, by the late stages of the evolution, there is little evidence for much gas. Little can be said about the temperature evolution, except that it appears to remain low (< 0.5 keV) throughout the merger.

A major problem with forming ellipticals from spirals is to account for the disappearance of the gas from the original spirals. Star formation is too inefficient a process to suppose that it is all converted into stars, and so the bulk is probably blown away by supernova explosions and stellar winds, and ultimately, galactic winds. We believe that we are seeing this ejected gas in X-rays, notably in the *Antennae*, Arp 220 and NGC 2623.

A great range of gaseous structures are observed within the sequence, and three fundamental (and chronological) questions need to be addressed; When and where does this gas ejection process start? What is the true nature of the huge one-sided structures seen in the ultraluminous systems? Why is there only marginal evidence for a hot halo in the remnants?

5.3.1 Early stages

Even in a pre-merger system such as the *Antennae*, a great deal of hot gas is seen, some of it being forcibly ejected from the system. What about still earlier systems? One would perhaps intuitively think that no ejection could occur before the galaxies first encounter each other (i.e. before Arp 270),

Figure 15. The evolution of the diffuse structures seen within the merging galaxy sample. Plotted are the temporal variations of the temperature (stars), the size (in terms of the maximum extent) (squares) and the values of $L_X(\text{diff})/L_B$ (diamonds). All values have been scaled to those of the *Antennae*. Upper limits are given by arrows. Two sets of points are given for Arp 220, one (the higher set) for the case where the southern source is assumed to be associated with Arp 220, one (the lower set), for the case where it is not. In the case of NGC 520, it proved impossible to extract any believable information regarding any diffuse component, and no values are plotted.

and this idea is strengthened by the modelling work of Mihos & Hernquist (1996) in which no significant star-formation occurs before merging galaxies first meet. Arp 270 appears to be at such an early stage in its encounter, it just may be on the verge of gaseous ejection. Remember that this system is at such an early starburst episode that, although star-formation is taking place at a level between that of typical normal and starburst spirals, it may be occurring well away from the nuclei, the gas not having had time yet to be compressed into the nuclear regions. Arp 242, at a later stage, is almost certainly ejecting hot gas into its halo. Its distance makes it difficult for us to say for sure, but its X-ray structure, and temperature, along with the coincidences of $H\alpha$ features, point towards ‘blowout’-type ejection taking place within this system.

5.3.2 Mid-stages

These ejections of hot gas are likely to grow as the merger progresses, as an increasing amount of gas is compressed into the nuclei, giving rise to more and more supernova explosions. How then do these gaseous structures appear at the peak of merger-induced activity? Arp 220 and NGC 2623 are very similar systems. Both are extremely bright, especially in the infrared and in the radio, and are members of the class of ultraluminous far-infrared galaxies (FIRGs) discovered by IRAS (Sanders et al. 1988b). Both appear to be at an evolutionary stage corresponding to the short (50–100 Myr) violent starburst period, seen in the Mihos & Hernquist (1996) simulations. At first glance, both appear very similar in the X-ray, with a large, soft, gaseous feature apparently connected to the galaxy, but situated some way from it, and a harder, more compact source centred on the galaxy itself. Furthermore, the same phenomenon is seen in *ROSAT* observations of a third violently merging, ultralu-

minus FIR galaxy, NGC 6240 (Fricke & Papaderos 1996). Again, in this galaxy, which is very similar to both Arp 220 and NGC 2623 in terms of its extreme luminosity and position in the merging evolution, a massive (~ 50 kpc), one-sided, diffuse feature is seen in the soft band image, whereas in the hard band image, only a point-like nuclear source is visible.

The similarities between these three systems strongly suggest that the large soft features are associated with the merging galaxies. On the other hand, as discussed in Section 4.5, there is evidence for a group of galaxies at $z \approx 0.09$ lying behind the soft feature in Arp 220. The properties of the diffuse X-ray emission from galaxy groups have been established over the past few years as a result of studies with *ROSAT* (Mulchaey et al. 1996, Ponman et al. 1996). The temperature of the hot gas is typically ~ 1 keV, and the luminosity (for $H_0 = 75$ km s $^{-1}$ Mpc $^{-1}$) ranges widely from 10^{40} erg s $^{-1}$ to 10^{43} erg s $^{-1}$, with a strong positive correlation with temperature. Unfortunately, as reported in Section 4.5, the spectral properties of the diffuse source in Arp 220 are not very well constrained. At the best fit temperature of ~ 0.5 keV, the derived luminosity of 2.9×10^{42} erg s $^{-1}$ would be very high for a group, but if $T \sim 1$ keV (as is allowed by the data) it would be quite reasonable. Hence the group hypothesis for the soft source cannot be ruled out by the available data.

We have a choice, then, between two coincidences. Either the source to the south of Arp 220 is a background group, in which case it is a remarkable coincidence that very similar features (with no sign of any background galaxies) are seen in the two similar systems NGC 2623 and NGC 6240, or the source is associated with Arp 220 itself, in which case (unless we are prepared to invoke non-cosmological redshifts) it must be a coincidence that there is a group, or at least a pair, of galaxies behind it.

One might hope, if these features are indeed galactic outflows, that one would see some corresponding emission from them at other wavelengths. In the case of NGC 2623, the soft X-ray source extends well outside the optical galaxy, but the H α +N II emission-line image (Armus, Heckman and Miley 1990) shows very little structure in the direction of this outflow. It is believed that both soft X-ray emission and optical line emission are produced by the shocking of cool clouds embedded in a hot wind, and most normal systems where hot outflows are believed to exist (e.g. NGC 253, M82) show X-ray and optical line emission features of reasonably similar size (see Heckman et al. 1993). Arp 220 is a case in point, its optical emission line halo, as discussed in Section 4.5, is approximately coincident with the smaller, east-west X-ray halo. Nothing is seen however, coincident with the huge southern extension.

What are these features? If they truly are hot gas ejected from the merger, then several questions arise. Why do they have no counterparts at other wavelengths? Why are they one-sided?

The Mihos & Hernquist (1996) simulations suggest that in a merger between two similar-sized, gas-rich, large-bulge systems (as we believe we have sampled here), *two*, quite different bursts of star-formation occur. The first occurs as the systems first meet each other (i.e. from Arp 270 to somewhere close to the Arp 220 epoch), and is of a comparatively low level (a level, in fact, similar to that of nearby star-

bursts, such as NGC 253 and M82), and lasts for a comparatively long time. The second starburst is far more intense, and lasts for an extremely short time (~ 50 Myr), occurring around the time of nuclear coalescence (our time zero), i.e. at the Arp 220/NGC 2623 epoch. This starburst is very different from those experienced by the earlier ‘approaching’ and ‘contact’ mergers.

Consider now the possible evolution. The first starburst, because of its similarity to M82-types, is likely to produce similar bipolar outflows, as are observed, both in the *Antennae* (Read et al. 1995), and in Arp 220 (Section 4.5; Heckman et al. 1996). Interestingly, however, in both cases, there is evidence that the ‘bipolar’ nature of these outflows has become distorted by the evolution of the merger (as discussed in Sections 4.3 and 4.5, and in Read et al. (1995) and Heckman et al. 1996)). An alternative explanation for their appearance may relate to the creation of ‘unipolar’ outflows, as discussed below.

Perhaps the strangest facet of the large, soft features seen in the most luminous systems is their unimodality. Why do the structures seen in Arp 220, NGC 2623 (and NGC 6240) appear only on one side of the system? The answer may lie in the fact that these systems are evolving rapidly. Mac Low & McCray (1988), using the Kompaneets (1960) (thin-shell) approximation, numerically modelled the growth of superbubbles: large thin shells of cold gas surrounding a hot pressurized interior – the progenitors of galactic winds – in various stratified atmospheres. Among their findings, they discovered that superbubbles blow out of the H I layer when they grow to a radius of between one and two scaleheights. The swept up shell then accelerates outwards and fragments, due to Rayleigh-Taylor instabilities, and the wind is then able to escape into the inter-galactic medium at velocities of several thousand km s $^{-1}$ (see Heckman et al. 1993).

However, Mac Low & McCray (1988) also find that these bubbles will blow out on *one side only* of a disc galaxy if their centres are more than 50–60 pc from the centre of the disc. Now, in a (relatively) dynamically stable system, such as M82 or NGC 253, the starburst is found to be very symmetrically positioned with respect to the galactic disc, and bipolar structures are seen in the X-ray (Watson, Stanger & Griffiths 1984; Fabbiano 1988; Pietsch 1992; Strickland, Ponman & Stevens 1997; Read et al. 1997). In a rapidly-evolving ultraluminous merging system such as Arp 220 or NGC 2623 however, the central burst is highly unlikely to be so centrally positioned with respect to the quickly-moving and highly distorted gaseous components. There will then be a *single* direction of steepest pressure gradient, along which the bubble will expand most rapidly, leading to a one-sided blowout.

It is also possible that this might apply to earlier systems within the present sample, as alluded to above. The distorted ‘bipolar’ structure seen in the *Antennae*, for instance (Section 4.3; Read et al. 1995), may not be a bipolar wind after all, but rather a pair of unipolar winds, one produced from the northern starburst, one from the southern. There is some evidence to support this, both in terms of the fact that the individual discs have become very distorted, and that the individual nuclear starbursts appear to be offset (see Read et al. 1995). The same could be also true in the case of the ‘double bubble’ structure seen in Arp 220.

Two individual unipolar winds, as opposed to one bipolar wind may have produced this structure.

Mean physical properties for these hot gas structures can be inferred from our spectral fits if we make some assumptions about the geometries of the emission. We have assumed that both the Arp 220 southern feature and the NGC 2623 feature are spherical in nature, on the basis of the fact that both the Arp 220 and the NGC 6240 feature (Fricke & Papaderos 1996) appear quite round (the NGC 2623 feature appears quite round also, though we are unsure whether it has been resolved with the PSPC (see Section 4.6)). This is the simplest assumption to make and indicates the largest volume over which the gas is likely to be distributed. Using the volumes derived for this ‘bubble’ model, the fitted emission measure $\eta n_e^2 V$ (where η is the ‘filling factor’ – the fraction of the total volume V which is occupied by the emitting gas) can be used to infer the mean electron density, n_e , and hence the total mass M_{gas} , thermal energy E_{th} and cooling time t_{cool} of the gas, and also the mass cooling rate \dot{M}_{cool} and adiabatic expansion timescale t_{exp} . These values for the Arp 220 southern feature and the NGC 2623 eastern feature are given in Table 13, along with, for comparison, the corresponding values for the *Antennae* corona (Read et al. 1995), and for the NGC 7252, assuming that entire integrated emission from NGC 7252 is in the form of a hot gaseous halo.

If, as we are assuming, we are seeing some sort of outflow within these ultraluminous systems, then if $\eta \approx 1$, they are presumably bubbles of gas at $2-6 \times 10^6$ K flowing out from the system. If this is the case however, this gas, unless some additional force is confining it, should expand at its sound speed (a few hundred km s⁻¹), which is too slow when compared to the size of these features (≈ 50 kpc) and the timescale of the starburst (≈ 50 Myr). Alternatively, the soft X-ray emission we see could arise from material, e.g. clouds, shock heated by a fast wind (see Heckman et al. 1993). Although this hypothesis is supported by recent theoretical modelling of starburst winds (e.g. Suckov et al. 1994), the actual value of the filling factor of the gas emitting in the *ROSAT* band, remains unclear, some simulations (e.g. Suchkov et al. 1994) predicting a low value, others (e.g. D.K.Strickland, private communication) predicting a high value. In the low filling factor case, the *ROSAT* band X-ray luminosity of the clouds should far exceed that of the wind fluid itself. In the high filling factor case, the wind fluid contributes a very significant fraction to the *ROSAT* band emission.

In contrast to the corona surrounding the *Antennae* galaxies, therefore, which appears to be bound to the system ($\eta \approx 1$; see Read et al. 1995), the offset features seen in Arp 220 and NGC 2623 are (like the *Antennae* outflows) likely to be due to a combination of dense clouds, shocked by a hot, fast unbound wind, and the wind fluid itself. Provided that this material does escape from the system, then the associated mass loss rates can be calculated from the inferred gas masses, if we assume a velocity for the material. This gives 140 (for Arp 220) and 50 (for NGC 2623) $\times \sqrt{\eta} v_{1000} M_{\odot} \text{ yr}^{-1}$, where v_{1000} is the velocity, in units of 1000 km s⁻¹. Similarly, the rate at which kinetic energy is lost can be estimated to be 4.8 (Arp 220) and 1.7 (NGC 2623) $\times 10^{43} \sqrt{\eta} v_{1000}^3 \text{ erg s}^{-1}$.

If η were ≈ 1 , i.e. if we were seeing the hot wind itself,

rather than shocked clouds with $\eta \ll 1$, then this mass-loss could remove a substantial amount of gas ($\sim 10^{10} M_{\odot}$) from the merger (a requirement, if these objects are to eventually resemble gas-poor ellipticals), even over the short starburst timescale of 50 – 100 My. Furthermore, the rate at which kinetic energy could be lost turns out to be quite comparable to the total inferred supernova luminosities of these systems (calculated using the method of Read & Ponman (1995)); 28 and $6 \times 10^{43} \text{ erg s}^{-1}$, respectively for Arp 220 and NGC 2623. Hence, if η were ≈ 1 , then almost all of the mass and around a quarter of the energy injected into these systems by supernovae could escape in the wind.

If η is substantially less than unity, the above results still stand, though they refer to the mass and energy lost in the clouds (provided, of course, they escape the system). This reduces the mass and energy loss rates calculated, but there is of course additional mass and energy loss associated with the wind fluid itself, which is invisible to *ROSAT*. Simulations (Suchkov et al. 1994; D.K.Strickland, private communication) appear to show though, that the lower density phases of the gas do not carry a significant fraction of the mass.

It is also interesting to compare the values calculated above with the total energy and mass deposition rates, calculated (as in Heckman et al. 1993) in terms of the starburst bolometric luminosity L_{bol} (which in the cases of Arp 220 and NGC 2623 we may assume is approximately equal to L_{FIR}). The energy deposition rates $\dot{E} = 8 \times 10^{42} L_{\text{bol},11} \text{ erg s}^{-1}$ (where $L_{\text{bol},11}$ is in units of $10^{11} L_{\odot}$), are 6.9 (Arp 220) and 1.5 (NGC 2623) $\times 10^{43} \text{ erg s}^{-1}$, and the mass deposition rates $\dot{M} = 3L_{\text{bol},11} M_{\odot} \text{ yr}^{-1}$, are 25.9 (Arp 220) and 5.8 (NGC 2623) $M_{\odot} \text{ yr}^{-1}$.

As a final point, note that in the above discussion, we have only considered the Arp 220 southern feature, not the northern ‘double-bubble’ emission. Inclusion of this emission into the analysis, i.e. performing the same calculations to the results of fitting the *total* ‘diffuse’ spectrum (see Section 4.5), gives rise to estimated gas masses and thermal energies almost a factor of two greater than those given in Table 13. Hence if this material is also escaping, it will approximately double the mass and energy loss rates discussed above.

5.4 Final stages

The X-ray properties of the end products of our evolution, NGC 7252 and AM 1146-270, are rather intriguing (even though we were only able to obtain an upper limit for AM 1146-270, it is still quite a restrictive limit). As discussed earlier, the X-ray luminosities of these systems are low compared to ellipticals in general, more consistent with field spirals than with ellipticals. Furthermore, when compared to ellipticals of the same optical luminosity, it appears that both galaxies may be relatively X-ray dim. This, combined with the fact that the *ROSAT* PSPC image of NGC 7252 (Fig. 11) shows little in the way of any extended halo emission, poses a problem.

In the previous two subsections, we have discussed the massive amounts of hot gas seen in the vicinity of these earlier interacting systems. The gas which is present in winds will leave the system on a short timescale, so the fact that these X-ray structures are not seen at the NGC 7252 epoch,

	NGC 4038/9	Arp 220	NGC 2623	NGC 7252
$\log L_X$ (erg s $^{-1}$)	40.61	41.15	40.57	40.73
T_X (keV)	0.36	0.50	0.20	0.43
n_e (cm $^{-3}$)	$0.0049 \times 1/\sqrt{\eta}$	$0.0047 \times 1/\sqrt{\eta}$	$0.0069 \times 1/\sqrt{\eta}$	$0.0105 \times 1/\sqrt{\eta}$
M_{gas} (M_{\odot})	$1.5 \times 10^9 \sqrt{\eta}$	$8.5 \times 10^9 \sqrt{\eta}$	$2.4 \times 10^9 \sqrt{\eta}$	$1.8 \times 10^9 \sqrt{\eta}$
E_{th} (erg)	$3.1 \times 10^{57} \sqrt{\eta}$	$2.5 \times 10^{58} \sqrt{\eta}$	$2.7 \times 10^{57} \sqrt{\eta}$	$4.4 \times 10^{57} \sqrt{\eta}$
t_{cool} (Myr)	$2410\sqrt{\eta}$	$5590\sqrt{\eta}$	$2290\sqrt{\eta}$	$2590\sqrt{\eta}$
M_{cool} (M_{\odot} yr $^{-1}$)	0.62	1.52	1.06	0.70
t_{exp} (Myr)	59	90	82	38

Table 13. Values of physical parameters for the diffuse gas (using a hemispherical bubble model; see text) seen in the NGC 4038/9 corona, the Arp 220 southern feature, the NGC 2623 eastern feature, and the NGC 7252 halo. η is the filling factor of the gas.

a Gyr or so later, is not too surprising. The gaseous corona seen in the *Antennae* however, is different (coronal structures such as that within the *Antennae* may exist within Arp 220 and NGC 2623 as well, though limitations on spatial resolution and on numbers of counts make it impossible to say). The *Antennae*'s coronal gas, given the fact that it appears largely bound, with η close to unity (Read et al. 1995), is likely to have a long cooling time, perhaps 1–2 Gyr, and hence such a gaseous halo should remain until the NGC 7252 epoch. This starburst generated gas may be the origin, as discussed earlier, of the hot gaseous halos known to exist around many large ellipticals (e.g. Fabbiano 1989). For this hypothesis to work, one would expect hot gaseous halos around merger remnants. Why then, given that there is a good deal of evidence that hot gas should remain around the system until after obvious morphological evidence of a merger has vanished, does NGC 7252, the prototypical merger remnant candidate, show little sign of a hot halo?

The problem is not in reconciling the observations of the earlier systems with those of NGC 7252. As can be seen from Table 13, the coronae seen in the *Antennae* and in NGC 7252 are very similar in terms of amount of gas. It is true though that, as the *Antennae* merger progresses through the ultraluminous phase, more energy and mass is likely to be injected into the halo, making it uncomfortably large when compared to the NGC 7252 X-ray observations. On the other hand cooling is taking place, returning the hot coronal gas to the disc, and over the 1.5 Gyr or so between the *Antennae* phase and the NGC 7252 phase, even at its present (relatively low) cooling rate, $10^9 M_{\odot}$ of material will have returned to the central system. The real problem is that, in order for the merger hypothesis to work, and in order for these merger remnants to resemble elliptical galaxies in the X-ray, the halos need to be far larger (~ 50 – 100 kpc), more massive ($\sim 10^9$ – $10^{10} M_{\odot}$; Fabbiano 1989; Forman et al. 1993) and hotter ($T \approx 0.7$ – 1.2 keV; Matsushita et al. 1994; Rangarajan et al. 1995) than that observed around the prototype remnant, NGC 7252.

The solution may be that we are looking for elliptical-like X-ray properties in merger remnants of far too young a dynamical age. For instance, it is thought that it will still take a few billion years for the optical luminosity, brightness distribution, colour gradients, velocity dispersion, UVB colours and fine structure (shells, loops, ripples etc.) of NGC 7252 to evolve to that consistent with a normal el-

liptical (Schweizer 1996). Perhaps it will take as long for the X-ray properties to do the same.

In remnants such as NGC 7252, quite a substantial amount of gas still remains, both in the tidal debris and in the central molecular disc. Hibbard & van Gorkom (1996) believe that NGC 7252 needs to get rid of half of its molecular gas and about 90% of its tidal material, in order to appear as an elliptical galaxy. The removal of the central molecular gas appears to present no real problem. What remains can be converted into stars within the next few Gyr, given current central star-formation rates (1 – $2 M_{\odot}$ yr $^{-1}$; Hibbard et al. 1994). The removal of the tidal debris however may be of particular interest. In a recent N-body simulation of NGC 7252 (Hibbard & Mihos 1995), it was seen that the majority of the material within the interaction-induced tidal tails is actually bound to the remnant. The bases of the tails fall back quickly, whereas the more distant material falls back more slowly. Some fraction of the material however may remain far from the remnant in very long tails, for very long times (e.g. 20% of the tidal material is believed to remain beyond 90 kpc for over a Hubble time). Although this material would be far too faint to observe, it may contribute to the Ly α forest and to the IGM (Hibbard & van Gorkom 1996). This return of the tidal debris therefore, can stretch out the merger remnant lifetime to many Gyr.

The fact that the atomic gas disappears rather abruptly at the base of NGC 7252's northwestern tail, a region where the H I gas is seen to be falling toward smaller radii, whereas the optical tail continues across the face of the galaxy, is very suggestive of a quick and efficient process taking place converting the infalling gas to other phases (Hibbard et al. 1994). One possibility as to what happens to the H I gas is that it is converted into molecular gas through compression, in which case the system will remain rich in molecular gas for a long time. The other possibility is far more attractive; this returning material may be shock heated by the hot, though at this epoch, small halo. As this process continues, the X-ray luminosity and size of this halo will grow. The accompanying injection of energy will also raise the temperature. This is perhaps how large, hot X-ray halos are formed around merger remnants, (a requirement for the success of the merger hypothesis). The main bulk of the halo is not formed through the ejection of hot gas from the merger during the starburst stages of the interaction, but is instead formed, much later, through the shock-heating of tidal tail material falling back onto the remnant. If this picture is cor-

rect, then it is not surprising that only a small X-ray halo exists around NGC 7252. There is still a long time to wait (a few Gyr) before the bulk of the tail material returns, forming the large X-ray halos seen around many ellipticals.

5.5 X-rays from tidal tails

There is much evidence for enhanced star-formation, and even dwarf galaxy formation, within merger induced tidal tails (e.g. Schweizer 1978; Schombert et al. 1990). It is known that large amounts of neutral hydrogen are found within such tails (e.g. van der Hulst 1979; Hibbard et al. 1994), and the self-gravity of this material can cause clumping, and lead eventually to star-formation. At the tip of the *Antennae*'s southern tail, for instance, Mirabel, Dottori & Lutz (1992) have discovered a dwarf galaxy in the process of forming. This feature however, a chain of nebulae ionized by very young (< 6 Myr) stars, is found to emit no significant X-ray emission (Read et al. 1995). This is not too surprising, given that, if all the stars have been formed within the last 6 Myr, even the most massive of these would not have had time to evolve off the main sequence into the X-ray bright supernova remnant or high-mass X-ray binary phase. In later systems, however, X-ray features may be visible, as stars may have had time to evolve to X-ray bright phases.

In practice, no significant emission is seen coincident with any tidal tail features anywhere within our merging galaxy sample. The soft diffuse feature seen to the west of NGC 2623, at first glance, may appear to have something to do with the western tail. However, as discussed in Section 4.6, this is very unlikely to be the case. Even in NGC 7252, a system showing several large clumps of gas within its tidal tails (Hibbard et al. 1994), no obvious X-ray counterparts are observed. A small amount of emission is seen however, within the eastern tail, spatially coincident with a giant H II region (Hibbard et al. 1994) – the bluest region within the whole of NGC 7252. This feature (the ‘plume’ of emission to the north of the source at $\alpha = 22h20m56.25s$, $\delta = -24d42m06.4s$) contains only ~ 7 counts however, and a 2σ upper limit to its (0.1–2.0 keV) luminosity (assuming a 5 keV bremsstrahlung model) is $L_X < 1.7 \times 10^{39}$ erg s $^{-1}$. Converting the optical luminosity of this H II region (1.8×10^{41} erg s $^{-1}$; Hibbard et al. 1994) into an X-ray luminosity, assuming a similar L_X/L_B ratio to NGC 7252 as a whole, gives $L_X = 1.7 \times 10^{38}$ erg s $^{-1}$, a factor of ten below our upper limit. It is not, therefore, surprising that we do not detect any significant X-ray emission from this region.

6 CONCLUSIONS

We have completed a programme of *ROSAT* PSPC and HRI observations of a carefully chosen chronological sequence of eight merging systems in order to study the evolution of their X-ray properties through the merging process. While we have discussed the X-ray emission from each individual system in some detail, our main conclusions pertain to the evolutionary sample as a whole, and these conclusions are outlined below:

- Across the sequence, from separated discs to relaxed

remnants, the activity level is seen to rise, from a level between that of nearby normal and starburst spirals, to a level far in excess of that of nearby starbursts, returning, at the end of the sequence to a level similar to that at the start.

- Large amounts of hot gas are seen being forcibly ejected from these systems, the quantities of gas, and their extents, increasing with activity. The gas ejection process starts soon after the galaxies first meet each other, and evolves into what appear to be bipolar ‘blowout’-type winds. These ‘bipolar’ features may be similar to those seen in nearby starbursts, the distortions due to the rapid evolution of the systems, or they may be due to two separate ‘unipolar’ winds, one ejected from each of the two interacting galaxies. What appear to be massive, unipolar, ejections of hot gas are observed at the ultraluminous phases of the interaction, at the point of nuclear coalescence. These may result from a far more violent starburst taking place at this phase than at earlier stages, combined with very fast and vigorous dynamical evolution of the system. At later times however, in the elliptical-like, relaxed remnant phase, almost all of this hot gas appears to have vanished, leaving only the suggestion of a small X-ray emitting halo.

- The X-ray luminosity evolution, like the general activity level, rises and falls along the evolutionary sequence. However, the amplitude of this change is considerably (more than an order of magnitude) smaller than that seen in the far-infrared. The resulting large drop in the L_X/L_{FIR} ratio is probably realted to the ejected hot gas. The FIR flux is primarily due to dust heated by massive stars within the starburst, and hence tracks the star formation history. However, the fraction of this energy which is radiated by hot gas is reduced as the starburst proceeds, as much of the input energy from supernovae and stellar winds actually goes into the kinetic energy of the ejected gas.

- The prototypical merger remnant NGC 7252, bears little resemblance to typical elliptical galaxies in the X-ray, a fact at first appearing to conflict with the ‘merger hypothesis’, whereby elliptical galaxies can be formed from the merger of two disc galaxies. One possible resolution of this problem is that we are looking at far too early an evolutionary age. Although NGC 7252’s X-ray halo is far smaller, less massive, less bright and cooler than those of typical ellipticals, shock heating of the returning tidal debris over the next few Gyr, may increasing the size, mass, luminosity and temperature of the halo. This may be the main source of an eventual elliptical-like X-ray halo, rather than the remnants of hot gas ejected into the halo at earlier phases.

- The observations of NGC 520 reveal that it has no discernable diffuse component, is very underluminous in the X-ray, and sits very uncomfortably in the X-ray evolutionary sequence. It appears from other multiwavelength studies, that the NGC 520 merger has left the disc intact, whether because of gas-poor progenitors or a low progenitor mass ratio, and is likely not to evolve into an elliptical galaxy.

ACKNOWLEDGEMENTS

AMR acknowledges the receipt of a SERC/PPARC studentship during the initial phases of this work, and the Royal Society for more recent support. Ray Wolstencroft was involved in the early stages of this work, and we would like

to thank him and also Ian Stevens, Dave Strickland and Duncan Forbes for valuable discussions. We thank Laurence Jones for optical observations of the *Antennae* and Arp 220 which have helped to clarify the nature of sources close to these systems. AMR also also acknowledges colleagues from the MPE *ROSAT* group for their support. This research has made use of data obtained from the UK *ROSAT* Data Archive Centre at the Department of Physics and Astronomy, Leicester University, UK. We also thank the referee for useful comments which have improved the paper. Data reduction and analysis was performed on the Starlink node at Birmingham.

REFERENCES

Amram P., Marcelin M., Boulesteix J., le Coarer E., 1992, *A&A*, 266, 106

Armus L., Heckman T.M., Miley G.K., 1990, *ApJ*, 364, 471

Armus L., Neugebauer G., Soifer B.T., Matthews K., 1995, preprint

Arp H., 1966, *Atlas of Interacting Galaxies*, California Institute of Technology

Arp H., in Hewitt A., Burbidge G., Fang L.Z., eds, *Observational Cosmology*, Dordrecht: Kluwer, p.502

Arp H.C., Madore B.F., 1987, *A Catalogue of Southern Peculiar Galaxies and Associations* (Cambridge Univ. Press)

Baan W.A., Haschick A.D., Buckley D., Schmeltz J.T., 1985, *ApJ*, 293, 394

Baan W.A., van Gorkom J., Schmelz J., Mirabel I.F., 1987, *ApJ*, 313, 102

Barnes J.E., 1988, *ApJ*, 331, 699

Barnes J.E., 1992, *ApJ*, 393, 484

Barnes J.E., Hernquist L., 1991, *ApJ*, 370, L65

Barnes J.E., Hernquist L., 1996, *ApJ*, 471, 115

Bernlöhr K., 1993, *A&A*, 270, 20

Borne K.D., Richstone D.O., 1991, *ApJ*, 369, 111

Branduardi-Raymont G., et al., 1994, *MNRAS*, 270, 947

Bregman J.N., Pildis R.A., 1994, *ApJ*, 420, 570

Bushouse H.A., Werner M.W., 1990, *ApJ*, 359, 72

Cash W., 1979, *ApJ*, 228, 939

Casoli F., Combes F., Dupraz C., Gerin M., Encrenaz P., Salez M., 1988, *A&A*, 192, L17

Casoli F., Dupraz C., Combes F., Kazes I., 1991, *A&A*, 251, 1

Cayatte V., Kotanyi C., Balkowski C., van Gorkom J.H., 1994, *AJ*, 107, 1003

Condon J.J., 1980, *ApJ*, 242, 894

Condon J.J., Broderick J.J., 1986, *AJ*, 92, 94

Condon J.J., Condon M.E., Gisler G., Puschell J.J., 1982, *ApJ*, 252, 102

Condon J.J., Helou G., Sanders D.B., Soifer B.T., 1990, *ApJS*, 73, 359

Davis L.E., Seaquist E.R., 1983, *ApJS*, 53, 269

de Vaucouleurs G., de Vaucouleurs A., Corwin H.G., Jr., 1976, *Second Reference Catalogue of Bright Galaxies (RCBG)*. University of Texas Press

de Vaucouleurs G., de Vaucouleurs A., Corwin H.G., Jr., Buta R.J., Paturel G., Fouqué P., 1991, *Third Reference Catalogue of Bright Galaxies (RC3)*. Springer-Verlag, New York

Devereux N.A., Eales S.A., 1989, *ApJ*, 340, 708

Dressler A., Gunn J.E., 1983, *ApJ*, 270, 7

Eales S.A., Arnaud K.A., 1988, *ApJ*, 324, 193

Evrard A.E., 1990, in Oegerle W.R., Fitchett M.J., Danly L., eds, *Clusters of Galaxies*. Cambridge University Press, Cambridge

Fabbiano G., 1988, *ApJ*, 330, 672

Fabbiano G., 1989, *ARA&A*, 27, 87

Fabbiano G., Trinchieri G., 1983, *ApJ*, 266, L5

Fabbiano G., Kim D.-W., Trinchieri G., 1992, *ApJS*, 80, 531

Fabbiano G., Schweizer F., Mackie G., 1996, *ApJ*, 478, 542

Forman W.R., Jones C., David L., Franx M., Makishima K., Ohashi T., 1993, *ApJ*, 418, L55

Fricke K.J., Papaderos P., 1996, in Zimmerman H.U., Trümper J.E., Yorke H., eds, *Röntgenstrahlung from the Universe*, MPE report 263, p.377

Fritze-von Alvensleben U., Gerhard O.E., 1994, 285, 775

Gull S.F., 1989, in Skilling J., ed, *Maximum entropy and Bayesian methods*. Kluwer Academic Press

Harwitt M., Houck J.R., Soifer B.T., Palumbo G.G.C., 1987, *ApJ*, 315, 28

Hasinger G., Turner T.J., George I.M., Boese G., 1992, OGIP calibration memo CAL/ROS/92-001

Heckman T.M., 1983, *ApJ*, 268, 628

Heckman T.M., 1993, in Schlegel E.M., Petre R., eds, *AIP Conference Proceedings 313: The Soft X-ray Cosmos*, AIP press, p139

Heckman T.M., Armus L., Miley G.K., 1987, *AJ*, 92, 276

Heckman T.M., Armus L., Miley G.K., 1990, *ApJS*, 74, 833

Heckman T.M., Lehnert M.D., Armus L., 1993, in Shull J.M., Thronson H.A., eds, *The Environment and Evolution of Galaxies*, Kluwer Academic Publishers

Heckman T.M., Dahlem M., Eales S.A., Fabbiano G., Weaver K., 1996, *ApJ*, 457, 616

Hernquist L., 1993, in Shull J.M., Thronson H.A., eds, *The Environment and Evolution of Galaxies*, Kluwer Academic Publishers

Hibbard J.E., Mihos J.C., 1995, *AJ*, 110, 140

Hibbard J.E., Guhathakurta P., van Gorkom J.H., Schweizer F., 1994, *AJ*, 107, 67

Hibbard J.E., van Gorkom J.H., 1996, *AJ*, 111, 655

Huang Z.P., Yin Q.F., Saslaw W.C., Heeschen D.S., 1994, 423, 614

Hubble E., 1936, *The Realm of the Nebulae*, Yale Univ. Press, New Haven

Hummel E., van der Hulst J.M., 1986, *A&A*, 155, 151

Jog C.J., Solomon P.M., 1992, *ApJ*, 387, 152

Joseph R.D., Wright G.S., 1985, *MNRAS*, 214, 87

Joy M., Harvey P.M., 1987, *ApJ*, 315, 480

Keel W.C., 1986, *ApJ*, 302, 296

Lake G., Dressler A., 1986, *ApJ*, 310, 605

Larson R.B., Tinsley B.M., 1978, *ApJ*, 219, 46

Lonsdale C.J., Diamond P.J., Smith H.E., Lonsdale C.J., 1994, *Nature*, 370, 117

Lynden-Bell D., 1967, *MNRAS*, 136, 101

Mackie G., Fabbiano G., 1997, in Arnaboldi M., Da Costa G.S., Saha P., eds, *The Second Stromlo Symposium: The Nature of Elliptical Galaxies*, ASP, San Francisco, p.1

Majewski S., Herald M., Koo D., Illingworth G., Heckman T.M., 1993, *ApJ*, 402, 125

Matsushita K., et al. 1994, *ApJ*, 436, L41

Mac Low M.-M., McCray R., 1988, *ApJ*, 324, 776

Mihos J.C., Hernquist L., 1994, *ApJ*, 431, L9

Mihos J.C., Hernquist L., 1996, *ApJ*, 464, 641

Mihos J.C., Bothun G.D., Richstone D.O., 1993, *ApJ*, 418, 82

Mirabel I.F., Dottori H., Lutz D., 1992, *A&A*, 256, L19

Mulchaey J.S., Davis D.S., Mushotzky R.F., Burstein D., 1996, *ApJ*, 456, 80

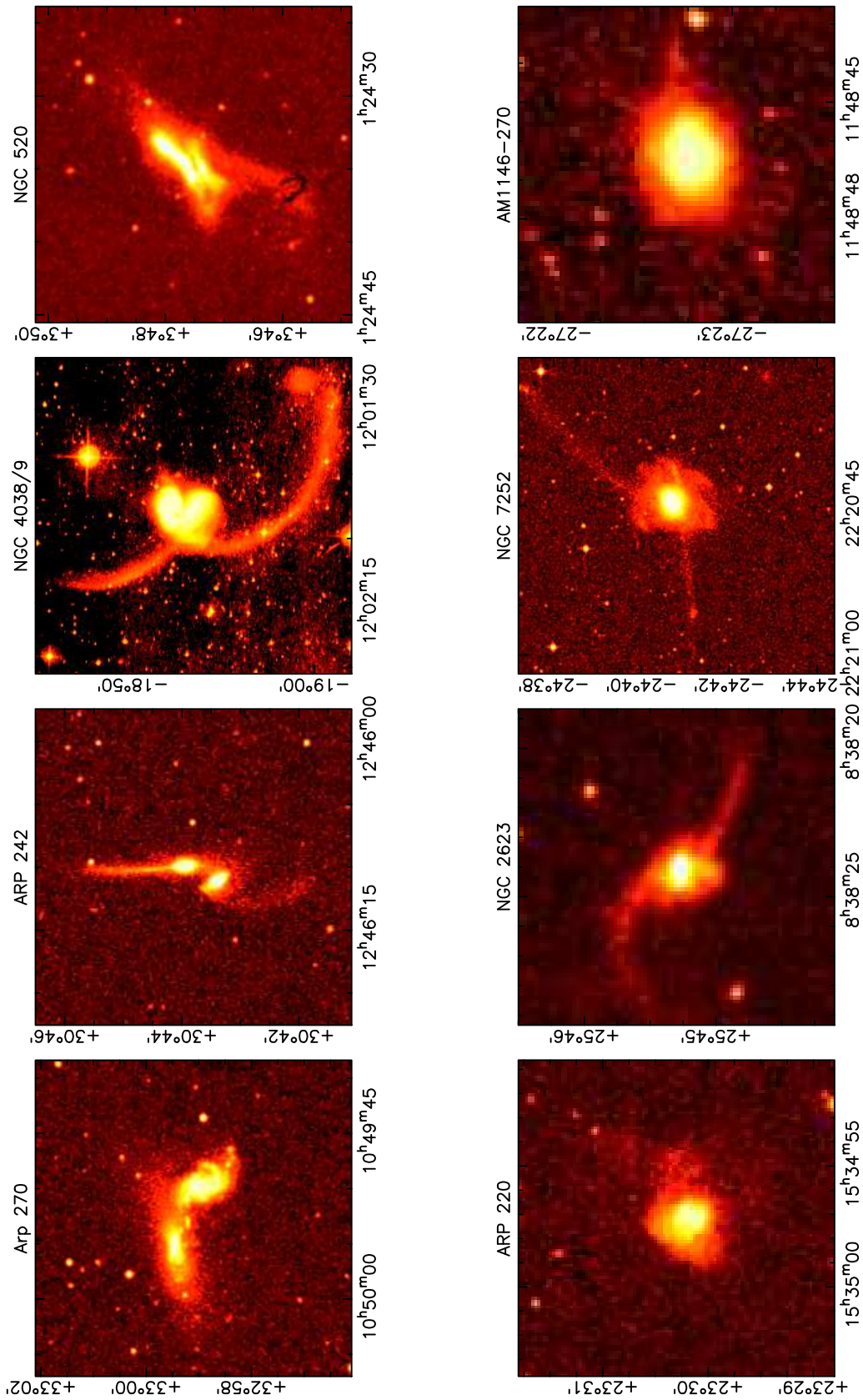
Petre R., 1993, in Beckman J., Colina L., Netzer H., eds, *The Nearest Active Galaxies*, Madrid:Consejo Superior de Investigaciones Científicas, p.117

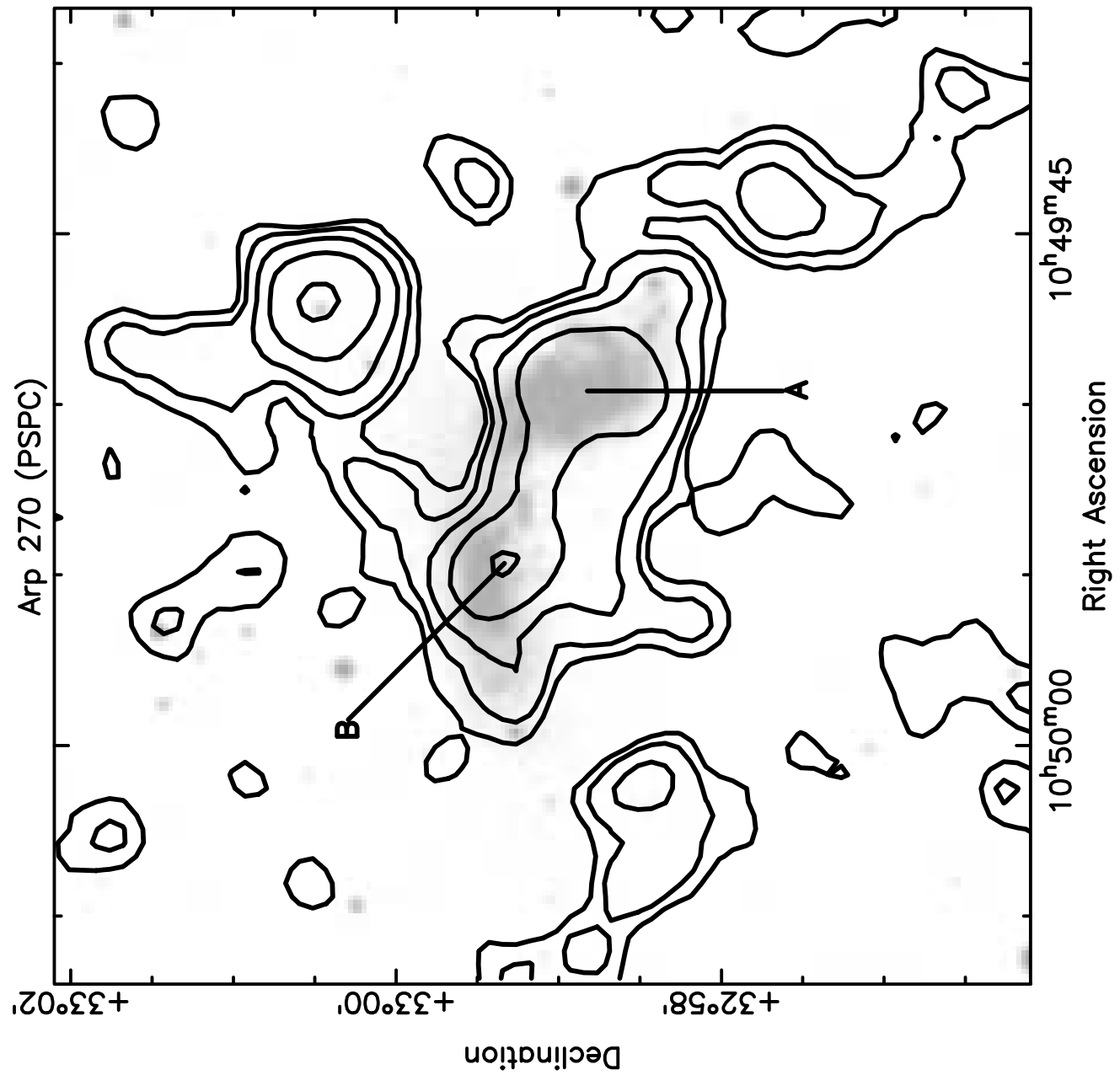
Pfeffermann E., et al. 1986, *Proc. SPIE*, 733, 519

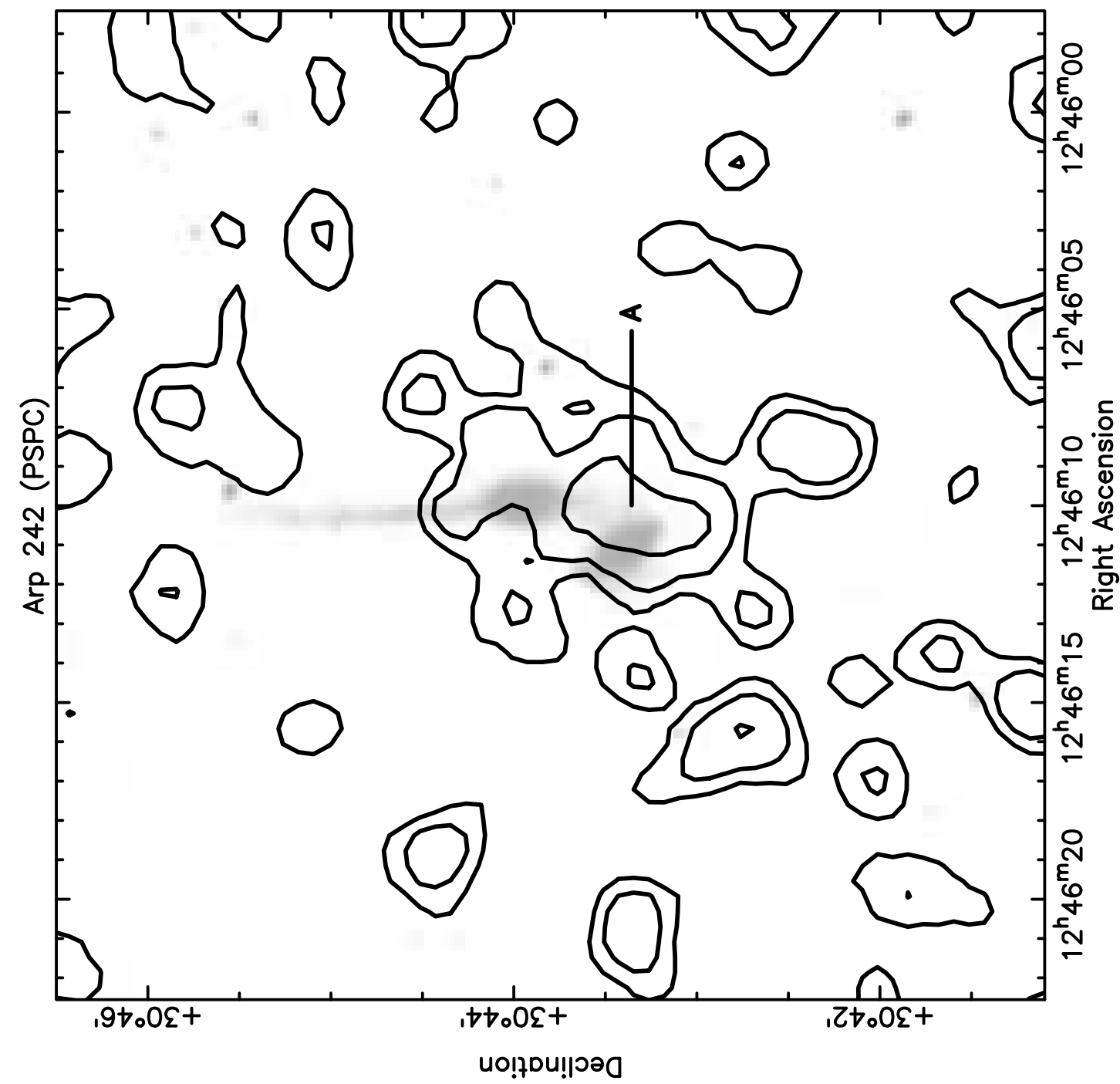
Pietsch W., 1992, in Thuan T.X., Balkowski C., Thanh Van J.T., eds, *Physics of Nearby Galaxies: Nature or Nurture?*, Editions Frontiers, France, p.76

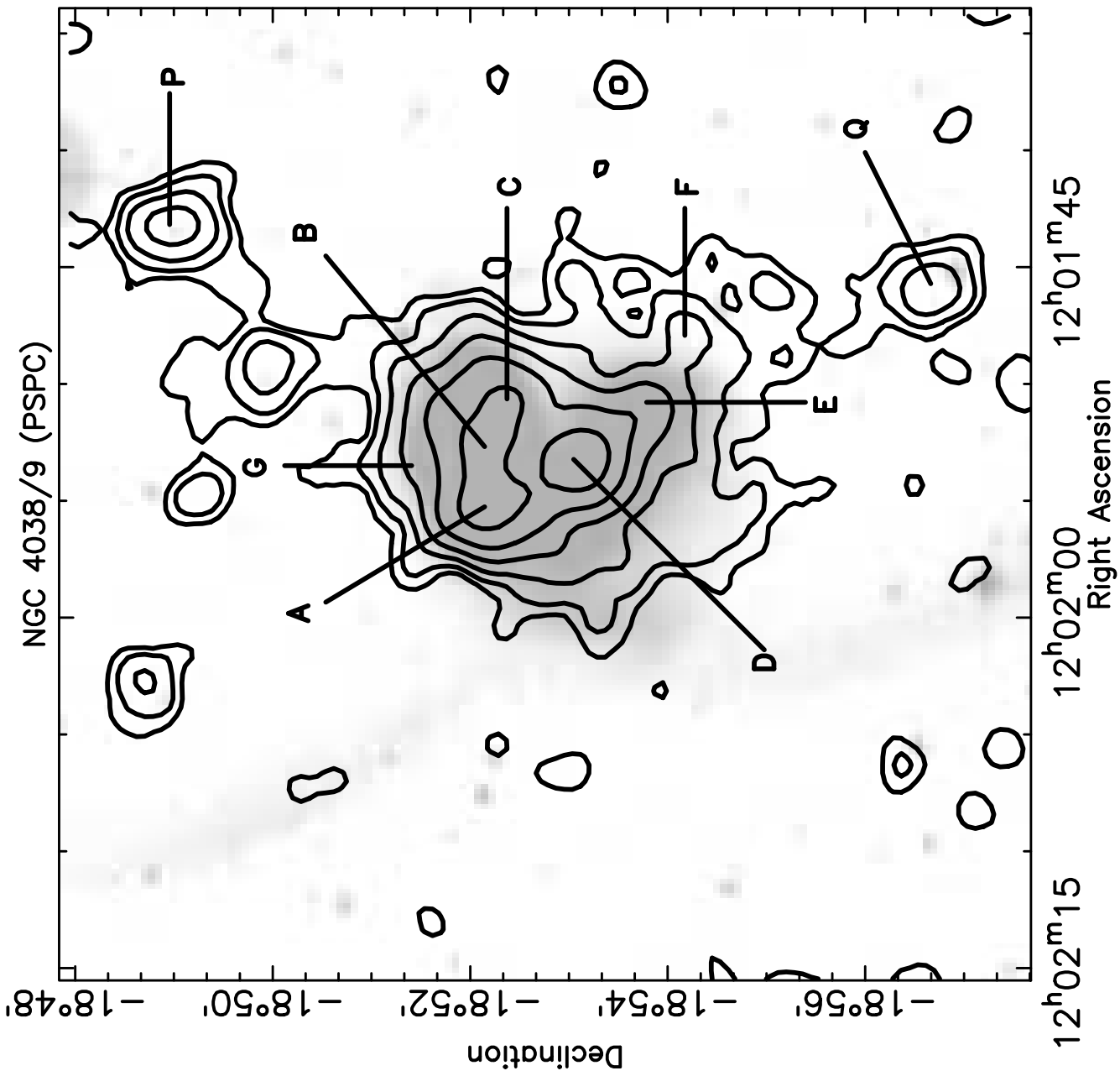
Ponman T.J., Bourner P.D.J., Ebeling H., Böhringer H., 1996, *MNRAS*, 283, 690

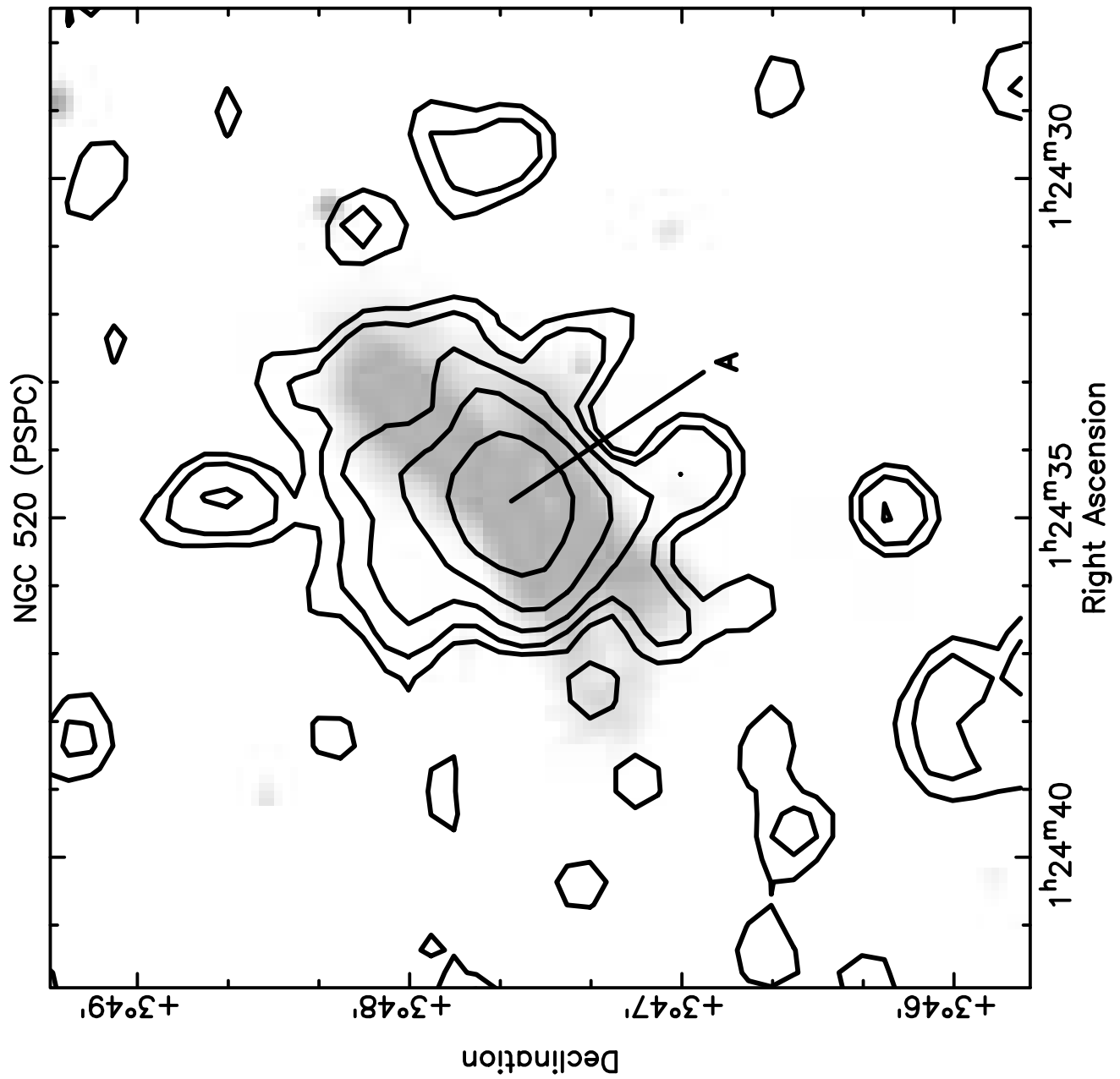
Prestwich A.H., Joseph R.D., Wright G.S., 1994, *ApJ*, 422, 73
 Quinn P.J., Hernquist L., Fullager D.P., 1993, *ApJ*, 403, 74
 Rangarajan F.V.N., Fabian A.C., Forman W.R., Jones C., 1995, *MNRAS*, in press
 Raymond J.C., Smith B.W., 1977, *ApJS*, 35, 419
 Read A.M., Ponman T.J., 1995, *MNRAS*, 276, 1327
 Read A.M., Ponman T.J., Strickland D.K., 1997, *MNRAS*, 286, 626
 Read A.M., Ponman T.J., Wolstencroft R.D., 1995, *MNRAS*, 277, 397
 Roche N., Shanks T., Georgantopoulos I., Stewart G.C., Boyle B.J., Griffiths R.E., 1995, *MNRAS*, 273, L15
 Rowan-Robinson M., Crawford J., 1989, *MNRAS*, 238, 523
 Rubin V., Ford W.K. Jr., D'odorico S., 1970, *ApJ*, 160, 801
 Sanders D.B., Scoville N.Z., Young J.S., Soifer B.T., Schloerb F.P., Rice W.L., Danielson G.E., 1986, *ApJ*, 305, L45
 Sanders D.B., Scoville N.Z., Sargent A.I., Soifer B.T., 1988a, *ApJ*, 324, L55
 Sanders D.B., Soifer B.T., Elias J.H., Madore B.F., Matthews K., Neugebauer G., Scoville N.Z., 1988b, *ApJ*, 325, 74
 Saslaw W.C., Valtonen M.J., Aarseth S.J., 1974, 190, 253
 Schombert J.M., Wallin J.F., Struck-Marcell C., 1990, *AJ*, 99, 497
 Schweizer F., 1978, in Berkhuijsen E.M., Wielebinski R., eds, *Structure and Properties of Nearby Galaxies*, Dordrecht: Reidel, p279
 Schweizer F., 1982, *ApJ*, 252, 455
 Schweizer F., 1986, *Science*, 231, 227
 Schweizer F., 1989, *Nat*, 338, 119
 Schweizer F., 1990, in Wielen R., ed, *Dynamics and Interactions of Galaxies*, Springer, Heidelberg), p60
 Schweizer F., 1996, *AJ*, 111, 109
 Scoville N., Soifer B.T., 1991, in Leitherer C., Walborn N., Norman C., Heackman T., eds, *Massive Stars in Starburst Galaxies*, Cambridge University Press p233
 Sekiguchi K., Wolstencroft R.D., *MNRAS*, 263, 349
 Skilling J., 1989, in Skilling J., ed, *Maximum entropy and Bayesian methods*. Kluwer Academic Press
 Smith E.P., Hintzen P., 1991, *AJ*, 101, 410
 Snowden S.L., McCammon, D., Burrows, D., Mendenhall, J., 1994, *ApJ*, 424, 714
 Soifer B.T., Sanders D.B., Madore B.F. Neugebauer, G. Danielson, G.E. Elias, J.H., Lonsdale C.J., Rice W.L., 1987, *ApJ*, 320, 238
 Solomon P.M., Sage L.J., 1988, *ApJ*, 334, 613
 Stanford S.A., 1991, *ApJ*, 381, 409
 Stanford S.A., Balcells 1990, *ApJ*, 355, 59
 Stanford S.A., Balcells M., 1991, *ApJ*, 370, 118
 Stanford S.A., Bushouse H.A., 1991, *ApJ*, 371, 92
 Stanford S.A., Sargent A.I., Sanders D.B., Scoville N.Z., 1990, *ApJ*, 349, 492
 Strickland D.K., Ponman T.J., Stevens I.R., 1997, *A&A*, 320, 378
 Suchkov A.A., Balsara D.S., Heckman T.M., Leitherer C., 1994, *ApJ*, 430, 511
 Takase B., Miyauchi-Isobe N., 1984, *Ann.Tokyo Astron.Obs.*, 2d Ser., 19, 595
 Telesco C.M., Wolstencroft R.D., Done C., 1988, *ApJ*, 329, 174
 Toomre A., 1977, in *Evolution of Galaxies and Stellar Populations*, Ed. B.M.Tinsley, R.B.Larson, p.401, (New Haven: Yale University Observatory)
 Toomre A., Toomre J., 1972, *ApJ*, 178, 623
 Tovmasyan H.M., Sramek R.A., 1976, *Afz*, 12, 21
 Tully R.B., 1988, *Nearby Galaxies Catalog*. Cambridge University Press, Cambridge
 van Albada T.S., 1982, *MNRAS*, 201, 939
 van der Hulst J.M., 1979, *A&A*, 71, 131
 Vigroux L., et al., 1996, *A&A*, 315, L96
 Wang Q.D., Walterbos R.A.M., Steakley M.F., Norman C.A., Braun R.A., 1995, *ApJ*, 439, 176
 Watson M.G., Stanger V., Griffiths R.E., 1984, *ApJ*, 286, 144
 Wevers B.H.M.R., van der Kruit P.C., Allen R.J., 1986, *A&AS*, 66, 505
 Wilson C.D., Elvis M., Lawrence A., Bland-Hawthorn J., 1992, *ApJ*, 391, L75
 Wolstencroft R.D., 1988, in Bertola F., Sulentic J.W., Madore B.F., eds, *New Ideas in Astronomy*. Cambridge University Press, Cambridge
 Wright G.S., James P.A., Joseph R.D., McLean I.S., 1990, *Nature*, 344, 417
 Young J.S., Knezec P.M., 1989, *ApJ*, 347, L55

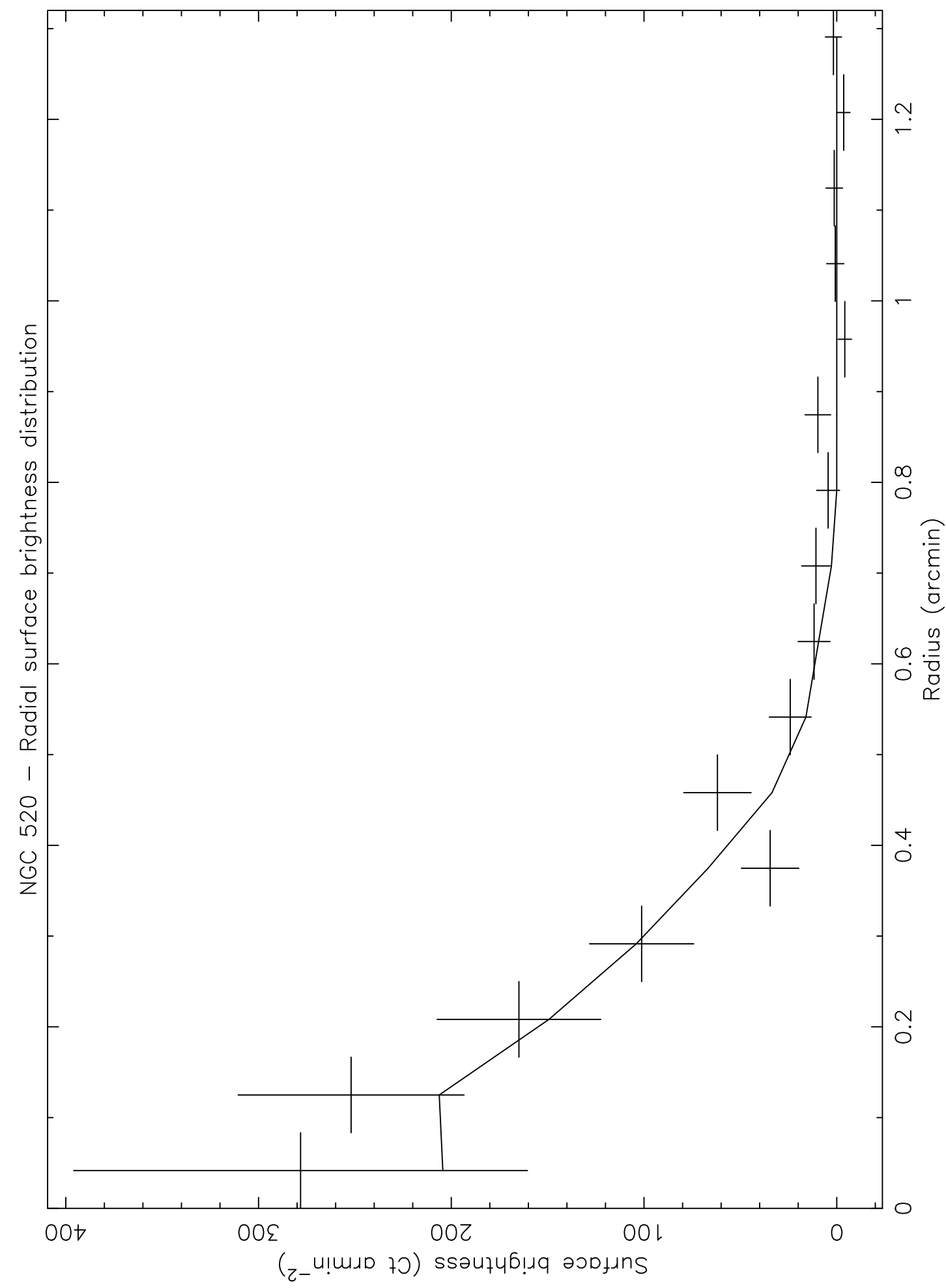


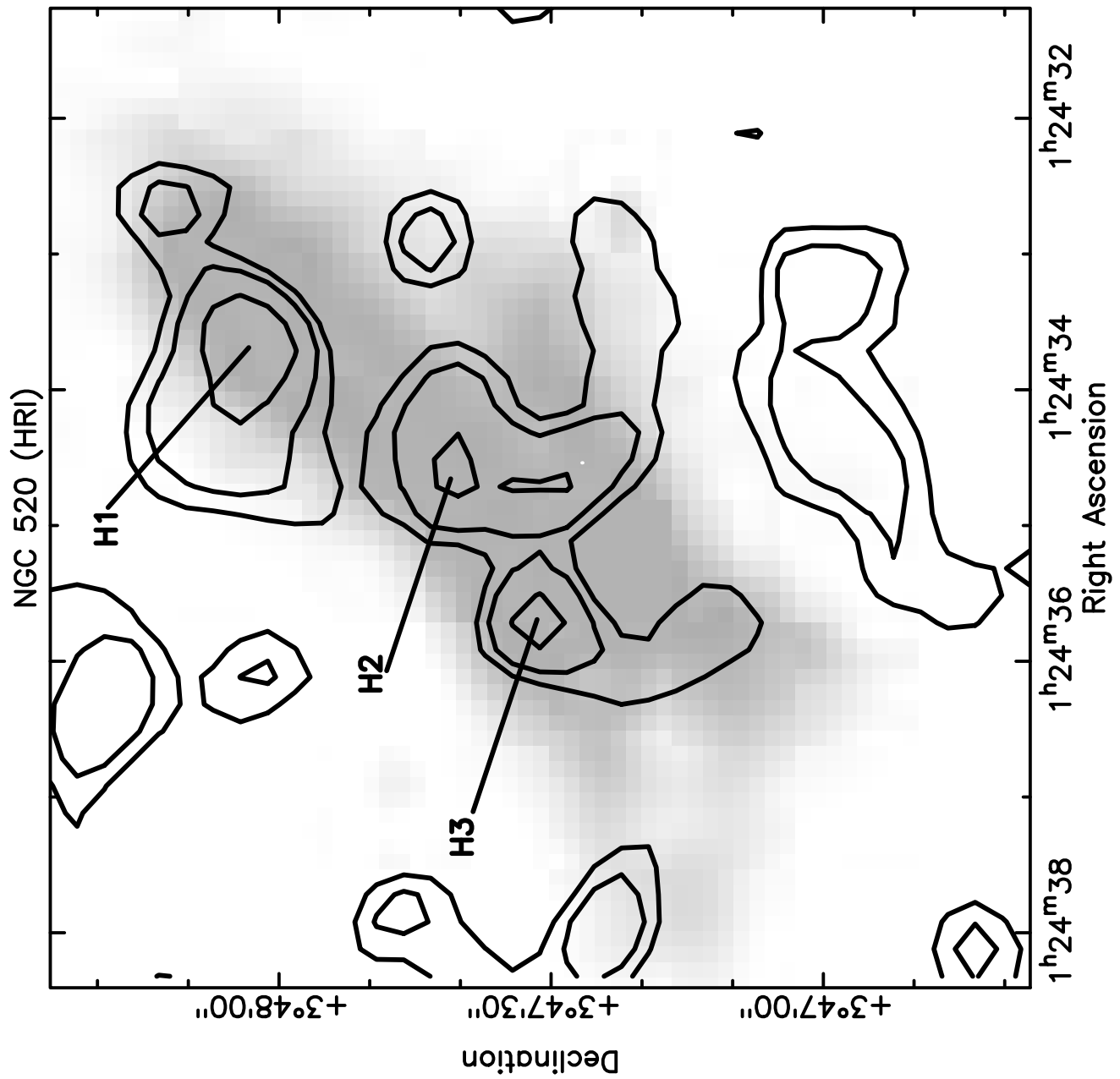


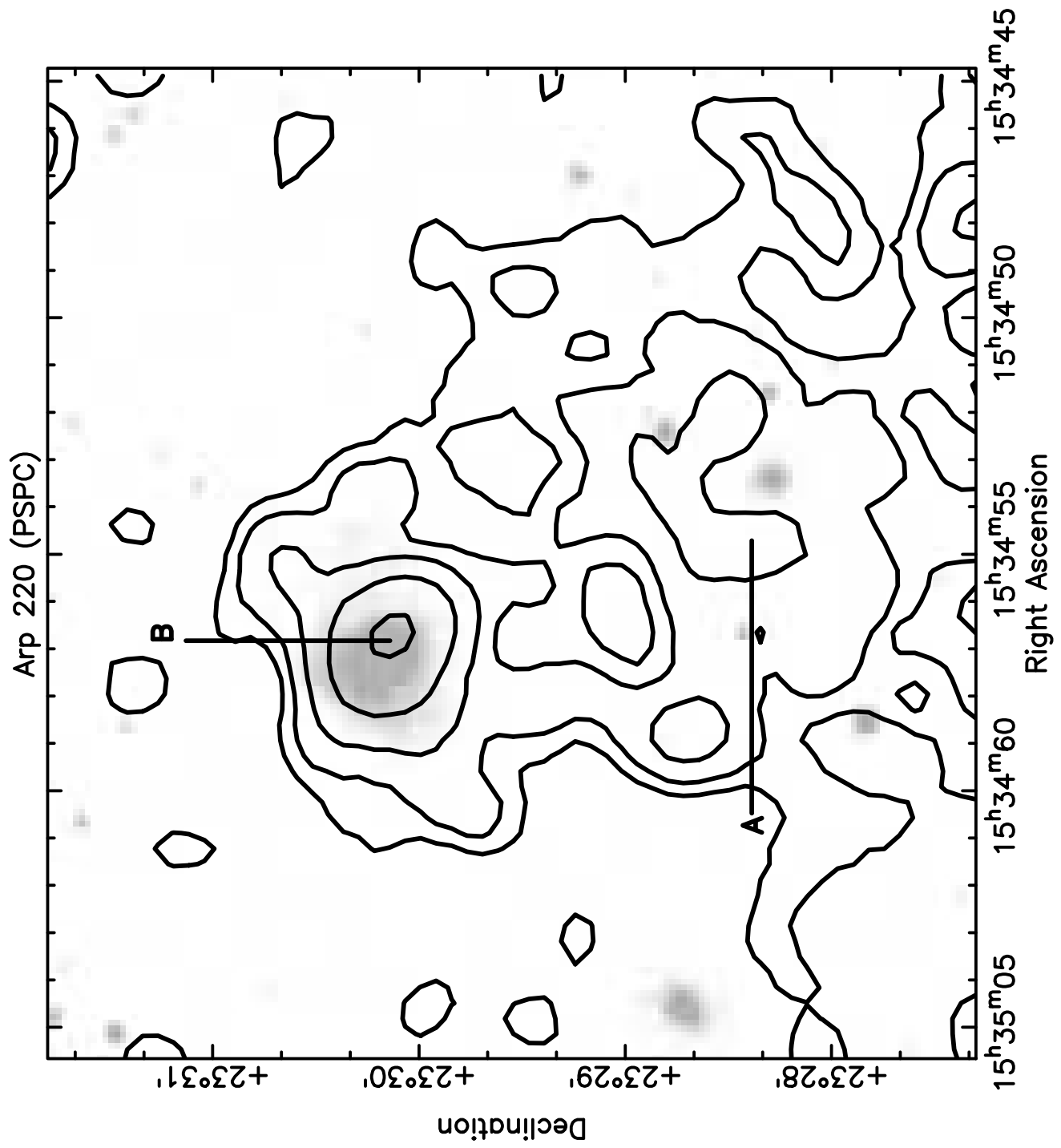












NGC 2623 (PSPC)

